

Heat Transfer and Fluid Flow Calculations of Industrial Shell Boilers and Evaluation of Operation Conditions – Draft

Saif-Aldain Aqel

2025



Budapest University of Technology and Economics

Faculty of Mechanical Engineering

Department of Energy Engineering

<http://www.energia.bme.hu/>

FINAL PROJECT ASSIGNMENT

Publicly Available

Identification	Name: Aqel Saif-Aldain Ahmad Deeb	ID: 73763256003
	Code of the Curriculum: 2NAAG0	Specialisation: 2NAAG0-PE
	Curriculum: Bachelor of Science Degree Program in Mechanical Engineering	Document ref. number: GEEN:2026-1:2NAAG0:QTY3S6
	Final Project issued by: Energetikai Gépek és Rendszerek Tanszék	Final exam organised by: Áramlástan Tanszék
	Supervisor: Dr. Lezsovits Ferenc (71957946594), associate professor	

Project Description	Title	Heat transfer and fluid flow calculations of industrial shell boilers and evaluation of operation conditions Nagyvízterű ipari kazánok hőátadási és folyadékáramlási számításai, valamint működési feltételek értékelése
	Details	1. Give an overview of application of shell boilers in industrial energy supply 2. Select a certain design of shell boilers for investigation and show its main data 3. Make combustion calculations considering gaseous and/or liquid fuel firing 4. Make heat transfer calculations for both fluegas and water-steam side 5. Make hydraulic calculations for both fluegas and water-steam side 6. Summarize all calculations and evaluate operation conditions of selected boiler 7. Make a sensitivity analysis of selected shell boiler on possible operation condition variations 8. Summarize all the results and evaluate them
	Advisor	Advisor's Affiliation: Advisor: ,

Final Exam	1 st subject (group)	2 nd subject (group)	3 rd subject (group)
	ZVEGEENBGHK Hőközlés	ZVEGEVGBX01 Áramlástechnikai gépek	ZVEGEENBGEB Energetikai folyamatok és berendezések

Authentication	Handed out: 8 September 2025	Deadline: 12 December 2025	
	Compiled by: Dr. Lezsovits Ferenc (71957946594) Supervisor	Verified by: Dr. Attila Imre (signed) Head of Department	Approved by: Dr. Gábor Györke (signed) Vice-Dean
	The undersigned declares that all prerequisites of the Final Project have been fully accomplished. Otherwise, the present assignment for the Final Project is to be considered invalid.		

Declarations

Declaration about the acceptability of the thesis

This thesis fulfills every formal and content requirements of the regulation of the Budapest University of Technology and Economics, moreover it fulfills the assignment of the final project. This thesis is suitable for a review and an open defense.

Budapest,

Dr. Lezsovits Ferenc

Declaration about the independent work

I, Saif-Aldain Ahmad Deeb Aqel (QTY3S6), hereby declare that the Thesis submitted for assessment and defense, exclusively contains the results of my own work assisted by my supervisor. Further to it, it is also stated that all other results taken from the technical literature or other sources are clearly identified and referred to according to copyright (footnotes/references are chapter and verse, and placed appropriately).

I accept that the scientific results presented in my Thesis can be utilized by the Department of the supervisor for further research or teaching purposes.

Budapest,

Saif-Aldain Aqel

Contents

Declarations	2
Table of Contents	4
List of Figures	5
List of Tables	6
Abstract	7
Nomenclature	8
1 Introduction	12
2 Industrial Application of Shell Boilers	15
2.1 Typical Industries	15
2.2 Standard Steam Duties	16
2.3 Advantages and Limitations	16
2.4 Multi-Pass Layout	18
3 Configuration	19
3.1 Layout	19
3.2 Geometry and surface specification	21
3.3 Assumptions and limitations	23
4 Combustion Model	24
4.1 Fuel and Air	25
4.1.1 Fuel Stream	25
4.1.2 Air Stream	25
4.1.3 Stoichiometric Oxygen requirement	26
4.1.4 Air-fuel ratio and excess air λ	27
4.2 Heating values and firing rate	28
4.2.1 HHV and LHV	28
4.2.2 Total heat input	29
4.3 Flame and flue gas	29
4.3.1 Methodology	30
4.3.2 Equilibrium flame state and adiabatic flame temperature	31
4.3.3 Boiler flue gas	31

5 Heat Transfer Model	32
5.1 Fundamental heat balance equations	32
5.2 Local energy balance	33
5.3 Overall conductance and resistance network	34
5.4 Wall temperature update and thermal convergence	35
5.5 Stage and boiler level duties	36
5.6 Gas side	36
5.6.1 Single tube and reversal chamber	37
5.6.2 Tube bank	38
5.6.3 Economizer	39
5.6.4 Radiation model	40
5.7 Water side	41
5.7.1 General formulation and boiling treatment	42
5.7.2 Economizer	45
5.7.3 Tube bank stages	47
5.7.4 Single tube and reversal chamber stages	48
6 Hydraulic Model	50
6.1 Frictional losses	50
6.2 Gas side pressure drop in the economizer	51
6.3 Minor losses	53
6.4 Total pressure drop	54
6.5 Coupling of ΔP into the energy solver	54
7 Performance	56
7.1 Solution procedure	56
7.2 Energy balance	57
7.3 Efficiency	57
7.4 Water/Steam flow rate convergence	58
8 Performance Analysis	59
8.1 Control case	59
8.1.1 Stage-wise heat transfer and hydraulics	60
8.2 Results and parametric analysis	62
8.2.1 Influence of excess air factor	62
8.2.2 Influence of fuel mass flow	65
8.2.3 Influence of drum pressure	67
8.2.4 Influence of fouling	69
8.3 Conclusions from performance analysis	70
9 Summary	73
A config and input	74
B Results summary	77
C Codebase	78
References	79

List of Figures

1.1	Shell boiler labeled stages (adapted from [12]).	13
1.2	$T-Q$ diagram for the three pass boiler with economizer.	13
2.1	Example of a packaged fire tube shell boiler in industrial service (reproduced from [4]).	15
3.1	Example of shell boiler setup components (reproduced from [4]).	19
3.2	Three-pass shell boiler with rear-mounted economizer for feedwater pre-heating (reproduced from [11]).	20
3.3	Detailed cross-section of the simulated boiler, showing drum, furnace, tube banks and reversal chambers (reproduced from [5]).	21
3.4	Cross-section of the economizer tube bundle HX_6 , showing gas-side cross-flow and water-side internal flow (reproduced from [6]).	22
4.1	Combustion flow	24
5.1	Cross section of heat transfer network from gas to water/steam	33
5.2	Path of flue gas through the 6 stages	37
5.3	Temperature–entropy ($T-s$) representation of the feedwater heating and evaporation process across economiser and boiler at the operating pressure (reproduced from [4]).	42
5.4	Path of water/steam through the 6 stages	45
8.1	Stage wise heat transfer and hydraulic profiles	61
8.2	Boiler performance as a function of excess air factor	63
8.3	Boiler performance as a function of fuel mass flow	65
8.4	Boiler performance as a function of drum pressure	67
8.5	Boiler performance as a function of fouling factor	69
8.6	Overview of key boiler performance indicators for all parameter groups .	71
8.7	Scatter diagram showing stack temperature and direct efficiency	72

List of Tables

3.1	Pool boiling pressure part geometry	22
4.1	Fuel composition in mass fractions. [3]	25
4.2	Air composition in mass fractions. [7]	26
4.3	Combustion reactions and stoichiometric factors	26
8.1	Control case performance.	59
8.2	Excess air performance analysis.	63
8.3	Fuel flow performance analysis.	66
8.4	Drum pressure performance analysis.	67
8.5	Fouling performance analysis.	70
A.1	Air parameters.	74
A.2	Drum parameters.	74
A.3	Fuel parameters.	75
A.4	Operation parameters.	75
A.5	Stages parameters.	75
A.6	Water parameters.	76

Abstract

This thesis develops a three pass fire tube industrial shell boiler model, implemented in Python, the modelling framework integrates (i) detailed fuel-air combustion, (ii) six sequential gas side heat exchange stages representing furnace, tube banks, reversal chambers, and economizer, and (iii) a water/steam circuit governed by saturated boiling in the pressure parts and single phase heating in the economizer. The gas–water energy balance is solved using a one dimensional marching algorithm, which updates local heat transfer coefficients, wall temperatures, and segmental duties based on a full resistance network.

Combustion calculations provide the adiabatic flame temperature, the fully burnt flue gas composition, and the total heat release the natural gas fuel provides. Hydraulic losses are resolved concurrently using friction factor and minor loss correlations yielding complete gas/water pressure drop profiles. Boiler level performance metrics, obtained under different operation conditions and analyzed, demonstrating that efficiency exhibits a shallow optimum near the design excess air setting; that pressure chiefly affects steam quantity rather than boiler efficiency; and that firing rate scales heat duties approximately linearly within the practical load range. The modelling framework provides a physics based tool suitable for analyzing industrial shell boiler behavior, supporting performance evaluation, operational optimization, and design exploration.

Nomenclature

Latin symbols

Symbol	Name	Units
A	Area	m^2
A_j	Gray-band weight	—
A_{bulk}	Bulk cross-flow area	m^2
$A_{\text{cold,flow}}$	Cold-side flow area	m^2
A_{flow}	Flow area	m^2
AFR	Air-fuel ratio	—
$A_{\text{hot,flow}}$	Hot-side flow area	m^2
B	Baffle spacing	m
C	Correlation coefficient	—
C_0	Bundle loss constant	—
D	Characteristic diameter	m
D_h	Hydraulic diameter	m
D_i	Inner diameter	m
D_o	Outer diameter	m
D_{shell}	Shell diameter	m
dx	Step length	m
f	Friction factor	—
F	View/enhancement factor	—
G	Mass flux	$\text{kg}, \text{m}^{-2}, \text{s}^{-1}$
Gz	Graetz number	—
h	Enthalpy / HTC	$\text{J}, \text{kg}^{-1} / \text{W}, \text{m}^{-2}, \text{K}^{-1}$
h_g	Gas-side HTC	$\text{W}, \text{m}^{-2}, \text{K}^{-1}$
HHV	Higher heating value	J, kg^{-1} (or $\text{J}, \text{mol}^{-1}$)
\dot{H}	Enthalpy rate	W
h_w	Water-side HTC	$\text{W}, \text{m}^{-2}, \text{K}^{-1}$
K	Loss/absorption coefficient	—
k	Thermal conductivity	$\text{W}, \text{m}^{-1}, \text{K}^{-1}$
K_j	Gray-band absorption	—
L	Length	m
L_b	Mean beam length	m
LHV	Lower heating value	J, kg^{-1} (or $\text{J}, \text{mol}^{-1}$)

Symbol	Name	Units
M	Molar mass	$\text{kg}, \text{mol}^{-1}$
M_{mix}	Mixture molar mass	$\text{kg}, \text{mol}^{-1}$
\dot{m}	Mass flow rate	kg, s^{-1}
M_w	Water molar mass	$\text{kg}, \text{mol}^{-1}$
n	Moles / exponent	$\text{mol} (\text{or } -)$
\dot{n}	Molar flow rate	$\text{mol}, \text{s}^{-1}$
N	Count	—
N_{rows}	Tube rows	—
Nu	Nusselt number	—
p	Pressure / partial pressure	Pa
P	Pressure	Pa
P_{LHV}	LHV firing rate	W
p_r	Reduced pressure	—
Pr	Prandtl number	—
Q	Heat rate	W
q	Dynamic pressure	Pa
$q'(x)$	Linear heat flux	W, m^{-1}
q''	Heat flux	W, m^{-2}
Q_{in}	Heat input	W
Q_{useful}	Useful heat	W
R	Thermal resistance / bend radius	—
Re	Reynolds number	—
R_p	Roughness parameter	μm
R'	Resistance per length	$\text{K}, \text{W}^{-1}, \text{m}^{-1}$
S	Suppression/pitch factor	—
S_L	Longitudinal pitch	m
S_T	Transverse pitch	m
T	Temperature	K
T_{ad}	Adiabatic flame temp.	K
T_{film}	Film temperature	K
T_{sat}	Saturation temperature	K
t	Wall thickness	m
τ_j	Optical thickness	—
UA	Overall conductance	W, K^{-1}
$UA'(x)$	Conductance per length	$\text{W}, \text{K}^{-1}, \text{m}^{-1}$
u_{max}	Velocity factor	—
V	Velocity	m, s^{-1}
w_i	Mass fraction	—
X	Mole fraction vector	—
x	Vapor quality / mole fraction	—
x	Axial coordinate	m
x_i	Mole fraction	—
X_{tt}	Martinelli parameter	—
y_i	Molar fraction	—

Symbol	Name	Units
ζ	Loss coefficient	—

Greek symbols

Symbol	Name	Units
α	Exponent/constant	—
ΔP	Pressure drop	Pa
ΔT	Temperature difference	K
δ	Thickness	m
ε	Emissivity / roughness	—
η	Efficiency	—
κ	Thermal conductivity	W,m ⁻¹ ,K ⁻¹
λ	Excess air ratio	—
μ	Dynamic viscosity	Pa,s
ν	Stoichiometric/kinematic viscosity	mol/mol (or m ² ,s ⁻¹)
Φ_{geom}	Geometry factor	—
ϕ	Correction/geometry factor	—
π	Pi	—
ρ	Density	kg,m ⁻³
σ	Stefan–Boltzmann constant	W,m ⁻² ,K ⁻⁴

Subscripts / indices / conventions

Index	Meaning	Units
ad	Adiabatic	—
air	Air	—
b	Bulk	—
bend	Bend	—
boiler	Boiler	—
c / cold	Cold side	—
conv	Convective	—
crit	Critical	—
drum	Drum	—
eq	Equilibrium	—
f	Saturated liquid	—
fg	Gas fouling	—
fo	Water fouling	—
fw	Feedwater	—
g	Gas side	—

Index	Meaning	Units
gw	Gas wall	—
HX_j	HX stage	—
in	Inlet	—
indirect	Indirect	—
l	Liquid	—
lo	Liquid-only	—
minor	Minor loss	—
nb	Nucleate boiling	—
out	Outlet	—
prod	Products	—
rad	Radiative	—
react	Reactants	—
ref	Reference	—
sens	Sensible	—
stage	Stage	—
steam	Steam	—
tot	Total	—
w	Water side	—
wall	Wall	—
ww	Water wall	—

Abbreviations

Abbrev.	Meaning	Units
AFR	Air–fuel ratio	—
API	Active pharmaceutical ingredient	—
CIP	Clean-in-place	—
HHV	Higher heating value	—
HP	Enthalpy–pressure mode	—
HTC	Heat-transfer coefficient	—
IAPWS-IF97	Water/steam properties standard	—
LHV	Lower heating value	—
NASA	Thermo data source	—

Chapter 1

Introduction

Industrial shell boilers remain one of the most widely deployed technologies for producing saturated steam and hot water in small to medium industrial plants. Their popularity arises from their compact construction, robust heat transfer surfaces, straightforward operation, and comparatively low installation and maintenance requirements. Typical applications span food and beverage processing, chemicals and pharmaceuticals, textiles, healthcare, and general manufacturing sectors where steady, reliable steam generation is essential for heating, processing, and auxiliary services.

Despite their apparent simplicity, the thermal behavior of shell boilers is governed by tightly coupled processes: multi stage radiative and convective heat transfer, natural circulation boiling inside the pressure parts, complex flue gas property variations, and geometry dependent hydraulic losses. Modern operation demands higher efficiency, reduced emissions, increased reliability, and improved control.

This thesis develops a physics based model for a three pass fire tube shell boiler that integrates combustion calculations, detailed flue gas thermophysical properties, multi stage heat transfer modelling, and hydraulic loss estimation. The model is implemented as a one dimensional marching solver applied to six sequential heat exchange stages;

$$HX_1 \rightarrow HX_2 \rightarrow HX_3 \rightarrow HX_4 \rightarrow HX_5 \rightarrow HX_6, \quad (1.1)$$

representing the furnace, reversal chambers, convective tube banks, and the economizer, see figure 1.1. On the water side, the boiler drum provides a saturated interface for nucleate boiling in the pressure parts, while the economizer section is treated as a single phase internal flow. Gas side properties are supplied by Cantera, enabling temperature dependent transport, specific heat, thermal conductivity, and radiative behavior to be modelled.

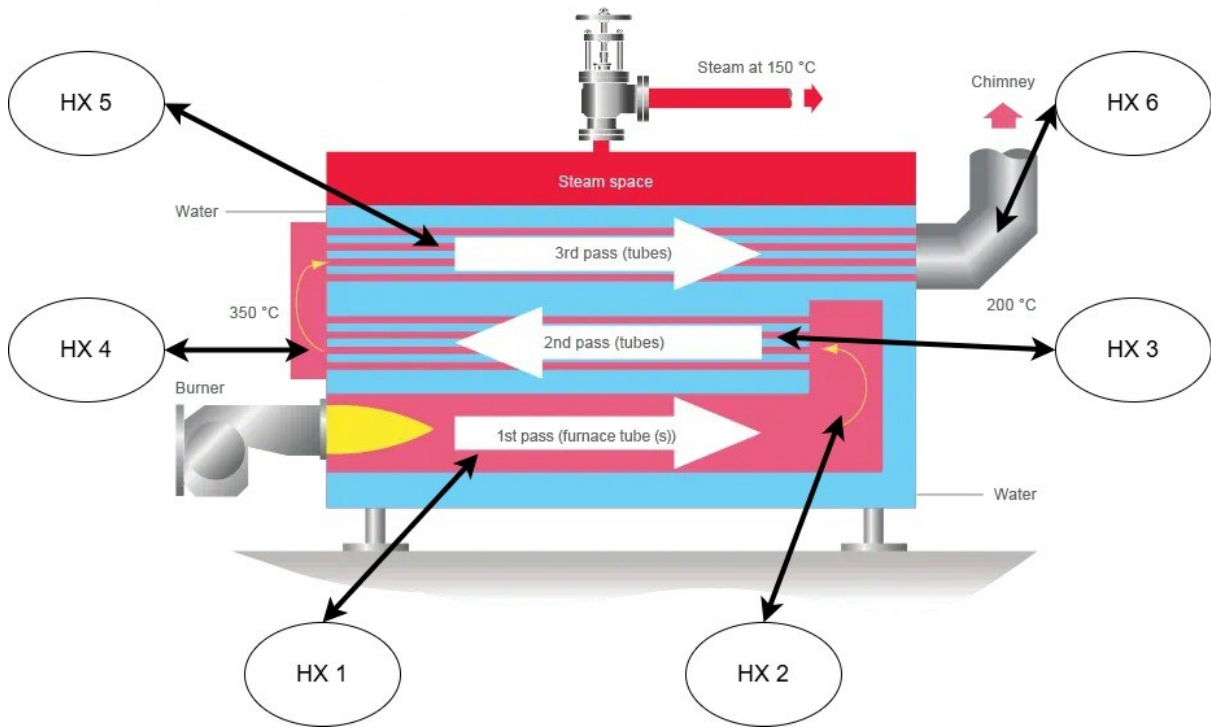


Figure 1.1: Shell boiler labeled stages (adapted from [12]).

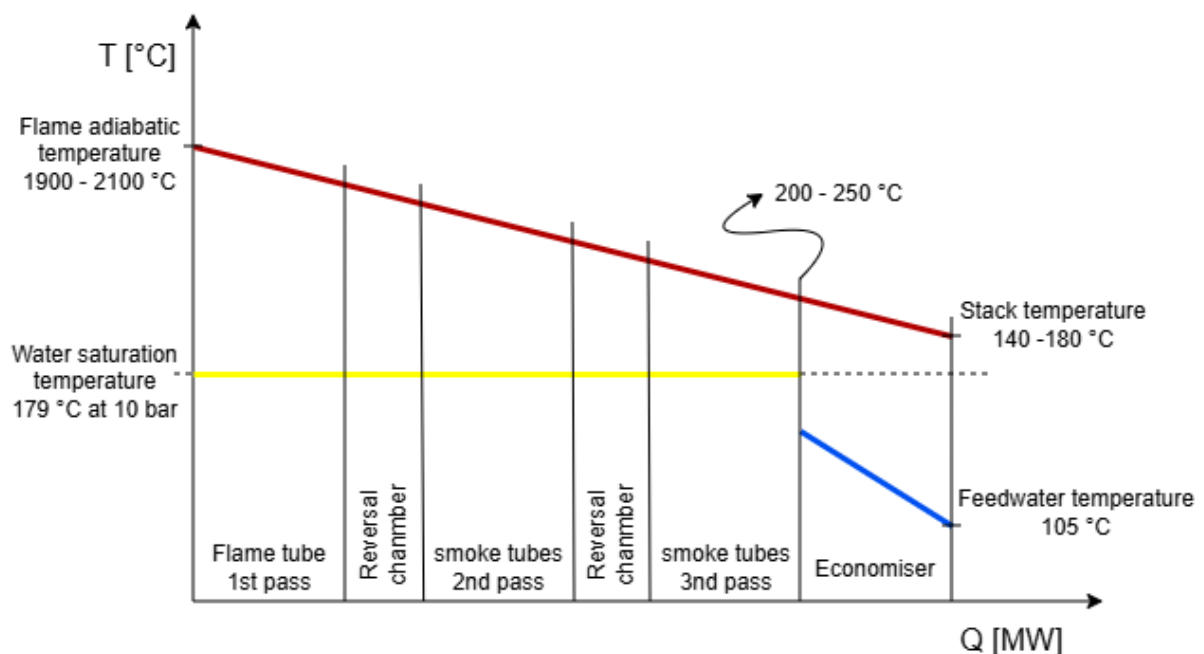


Figure 1.2: $T-Q$ diagram for the three pass boiler with economizer.

The overall objectives of the study are:

1. To construct a unified combustion-boiler model capable of predicting flue gas temperature, composition, adiabatic flame temperature, and total heat input based on fuel composition and excess air settings.

2. To resolve heat transfer processes along the boiler using stage specific geometries, convection correlations, and a spectral based gas radiation model.
3. To quantify hydraulic losses across each pass using friction factor relations and minor loss coefficients, yielding the total boiler gas side pressure drop.
4. To compute boiler level performance, including useful heat transfer, direct and indirect efficiencies, stack temperature, and stage wise duties.
5. To evaluate sensitivity of boiler performance to key operating parameters, excess air ratio, drum pressure, and fuel mass flow rate.

The numerical framework is structured such that the water/steam mass flow is determined iteratively from the global energy balance. For each operating condition, a fixed point loop between assumed efficiency and resulting steam flow is solved until convergence, ensuring consistency between combustion input, heat transfer output, and steam generation.

The remainder of this thesis is organized as follows. Chapter 2 identifies typical industrial applications of shell boilers and introduces key design features. Chapter 3 describes the boiler geometry and outlines the six heat transfer stages. Chapter 4 develops the combustion and flue gas model, including stoichiometry and adiabatic flame temperature prediction. Chapter 5 covers the heat transfer framework, combining convection and radiation on the gas side with pool boiling and single phase correlations on the water side. Chapter 6 presents the hydraulic model. Chapter 7 reports the resulting boiler performance, while Chapter 8 examines the sensitivity of the system to variations in λ , pressure, and firing rate. Chapter 9 concludes with a summary of findings.

Chapter 2

Industrial Application of Shell Boilers

Fire tube boilers- shell boilers

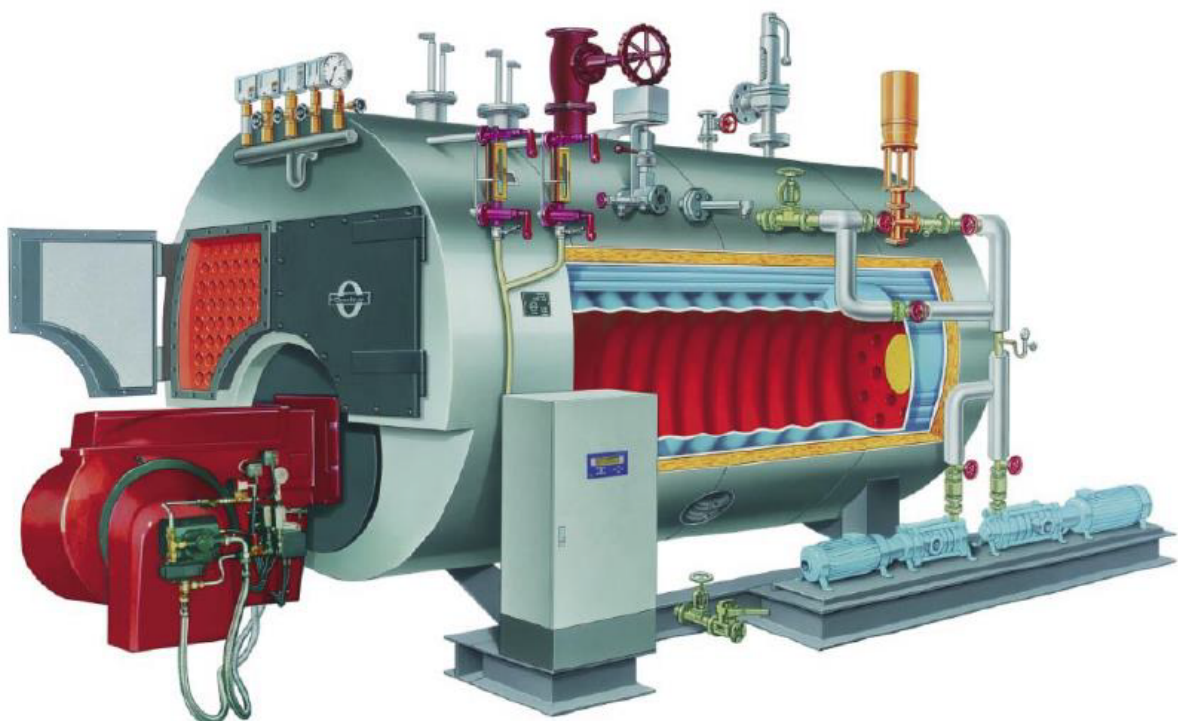


Figure 2.1: Example of a packaged fire tube shell boiler in industrial service (reproduced from [4]).

2.1 Typical Industries

Shell (fire tube) boilers are widely used in small to medium steam and hot water duties where compactness, robustness, and simple operation are prioritized over very high pressure or very large throughput. Typical sectors include:

- Food and beverage
 - Breweries, dairies, sugar refineries
 - Canneries, bakeries, confectionery plants
 - CIP (clean-in-place) systems and sterilization
- Chemical and pharmaceutical
 - Fine chemicals, specialty chemicals
 - Active pharmaceutical ingredient (API) and formulation plants
 - Steam for reactors, jacket heating, and clean steam generators
- Textiles and paper
 - Dyeing, washing, drying, and calendaring operations
 - Small paper mills and converting facilities
- Healthcare and institutional
 - Hospitals, clinics, and laboratories (space heating, humidification, sterilizers, autoclaves)
 - Universities, office complexes, district heating sub-plants
- Light manufacturing and general industry
 - Metal finishing, surface treatment, and cleaning
 - Rubber and plastics processing
 - Laundry services and commercial dry-cleaning

2.2 Standard Steam Duties

Shell boilers are normally applied in low to medium pressure ranges and moderate steam capacities:

- Typical operating pressure range:
 - Saturated steam: 6–25 bar, occasionally up to 30 bar
 - Hot-water service: 10–16 bar
- Steam-generation rates (order of magnitude):
 - Small units: 0.5–5 t/h
 - Medium units: 5–20 t/h
 - Large shell boilers (upper practical range): 20–40 t/h, beyond which water-tube designs are usually preferred

2.3 Advantages and Limitations

Advantages

- Compact and integrated construction

- Furnace, passes, and steam/water space are combined in a single pressure body.
 - Relatively small footprint and simple installation.
- Operational simplicity
 - Straightforward start-up and shutdown procedures.
 - Typically tolerant of moderate load swings and cycling (within design limits).
 - Often delivered as packaged units with burner, controls, and safety devices pre-engineered.
- Low-to-moderate capital cost
 - Attractive for small and medium plants, boiler houses, and decentralized steam supply.
- Good part-load performance
 - Large water content provides thermal buffer, reducing short-cycling of the burner.
 - Reasonable efficiency across a wide load range, especially with economizers.
- Maintenance and inspection
 - Accessible gas passes and tube bundles (depending on design) for cleaning and inspection.
 - Long-established technology with wide service and parts availability.

Limitations

- Pressure and capacity limits
 - Practical upper bounds on shell diameter and plate thickness limit maximum pressure and steam rate.
 - For very high pressure (e.g., >40–60 bar) or very large capacities, water-tube boilers are more suitable.
- Response time
 - Large water inventory slows thermal response to rapid, large load changes compared with water-tube boilers.
- Efficiency ceiling
 - Radiative and convective heat-transfer surfaces are constrained by geometry.
 - Very high efficiencies often require additional heat-recovery equipment (economizers, condensing stages, air preheaters).
- Transport and installation constraints
 - Shell diameter and weight can be limited by route and lifting capacity.
 - Retrofitting within existing boiler houses may be constrained by overall envelope.

2.4 Multi-Pass Layout

Industrial shell boilers typically adopt multi-pass fire-tube configurations to enhance convective heat transfer and maintain acceptable gas-side velocities:

- Two-pass layout
 - First pass: large diameter furnace tube running from burner front to rear reversal chamber.
 - Second pass: return of flue gas through banks of small-diameter fire-tubes back to the front reversal chamber and flue outlet.
 - Simpler construction but lower total heat-transfer surface compared with three-pass designs.
- Three-pass layout (most common for industrial shell boilers)
 - Pass 1: large diameter furnace tube running from burner front to rear reversal chamber.
 - Pass 2: First bank of smoke-tubes (typically reversing at the rear turnaround chamber).
 - Pass 3: Second bank of smoke-tubes.
 - Provides higher overall heat-transfer surface, more uniform gas cooling, and lower exit-gas temperatures.
- Extended heat-recovery sections
 - Economizer: additional convective heat exchanger in the flue-gas path downstream of the boiler to preheat feedwater.
 - Air preheater / condensing sections: for high-efficiency systems using suitable fuels and materials.
- Flow arrangement
 - Gas-side: burner → furnace (Pass 1) → turnaround chamber → tube bank(s) (Passes 2 and 3) → stack.
 - Water/steam side: natural circulation between heated tube surfaces and the upper steam space within the drum/shell; feedwater introduced at cooler regions (often via economizer), steam drawn from the top of the shell.

This multi-pass concept underpins the subsequent detailed modelling of each convective and radiative heat-transfer stage HX_1-HX_6 in the simulation.

Chapter 3

Configuration

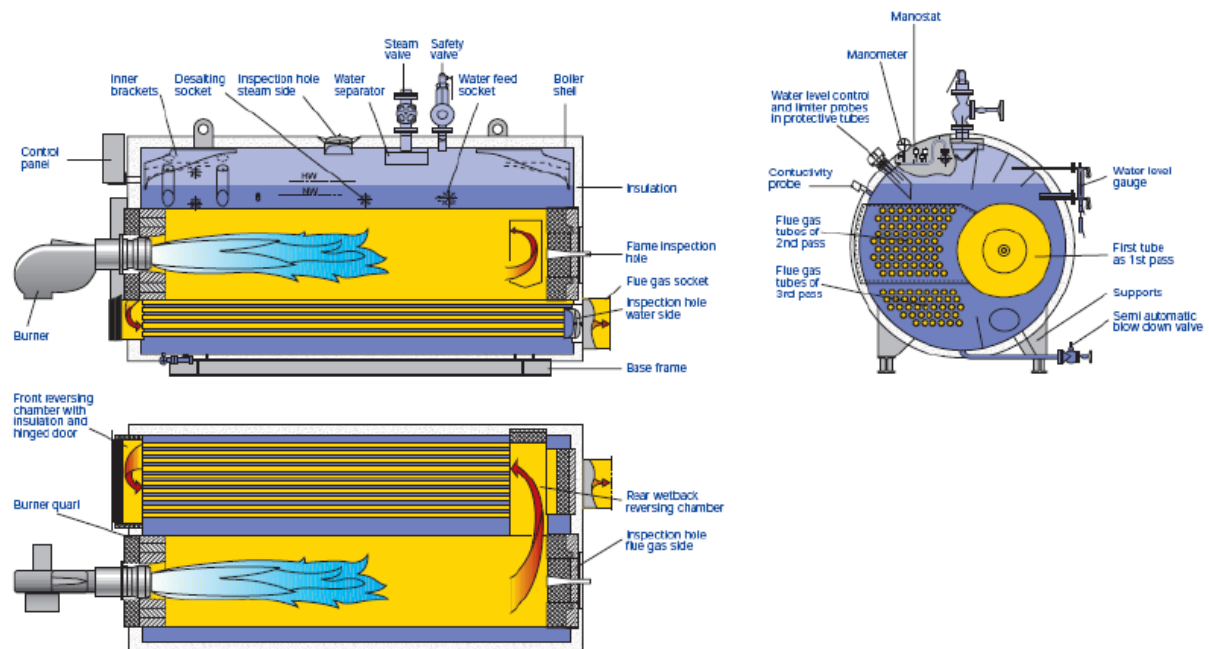


Figure 3.1: Example of shell boiler setup components (reproduced from [4]).

The simulated unit is a three pass fire tube shell boiler with six distinct gas side heat transfer stages and a single common steam drum on the water/steam side. Hot flue gas from the burner traverses a radiative furnace, two reversal chambers, two convective tube banks, and a final economizer before leaving to the stack.

3.1 Layout

The gas path is represented as:

$$\text{Burner} \rightarrow \text{HX}_1 \rightarrow \text{HX}_2 \rightarrow \text{HX}_3 \rightarrow \text{HX}_4 \rightarrow \text{HX}_5 \rightarrow \text{HX}_6 \rightarrow \text{stack} \quad (3.1)$$

with the following interpretation:

- HX_1 – Furnace (first pass)
Large, single furnace tube where combustion products enter directly from the burner and transfer heat mainly by radiation and high-temperature convection to the surrounding water/steam.
- HX_2 – First reversal chamber
Short cylindrical wet back chamber that turns the flow from the furnace outlet into the first convective tube bank (gas direction change = 180°).
- HX_3 – First convective tube bank (second pass) Bank of small diameter fire tubes arranged in a staggered pattern inside the shell, to boost convection; flue gas flows inside of the tubes, water/steam outside.
- HX_4 – Second reversal chamber Second turning chamber redirecting gas from the first to the second tube bank.
- HX_5 – Second convective tube bank (third pass) Second fire-tube bundle, representing the last in-boiler convective pass.
- HX_6 – Economizer Separate, downstream tube bank used to preheat feedwater in single-phase operation before entering the drum/boiler circuit, recovering heat, and boosting efficiency of the boiler.

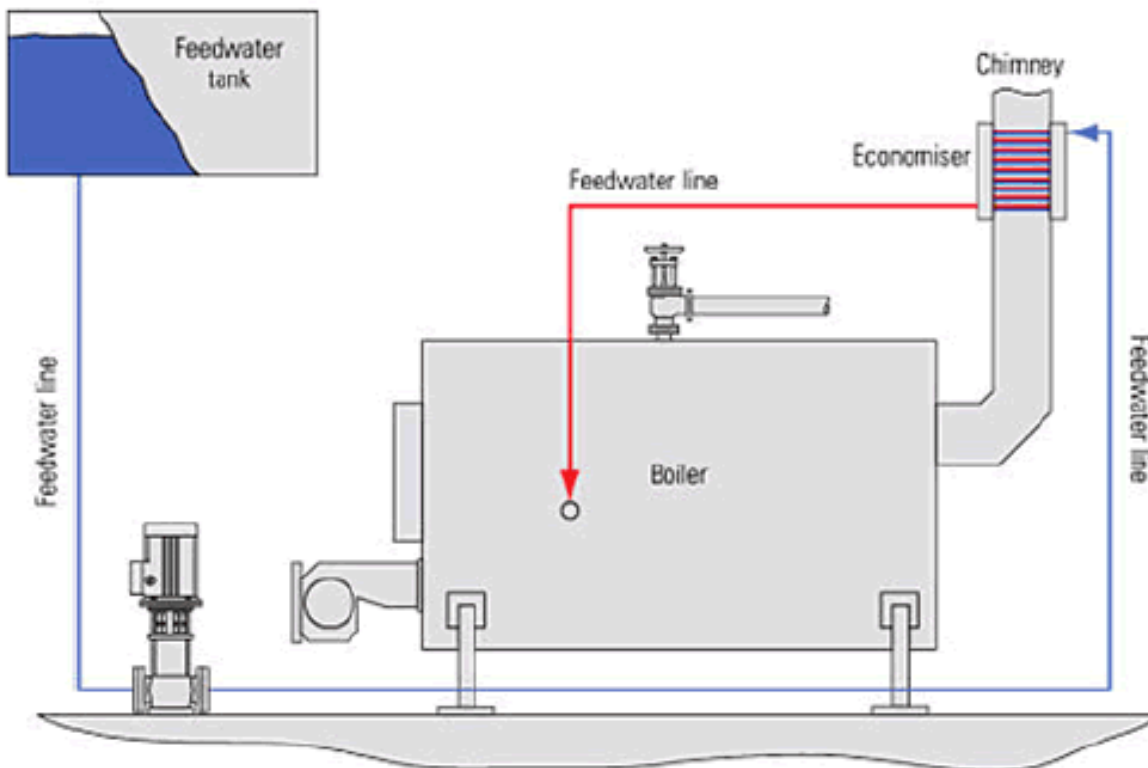


Figure 1: Economizer in Fire Tube Steam Boiler.

Figure 3.2: Three-pass shell boiler with rear-mounted economizer for feedwater pre-heating (reproduced from [11]).

3.2 Geometry and surface specification

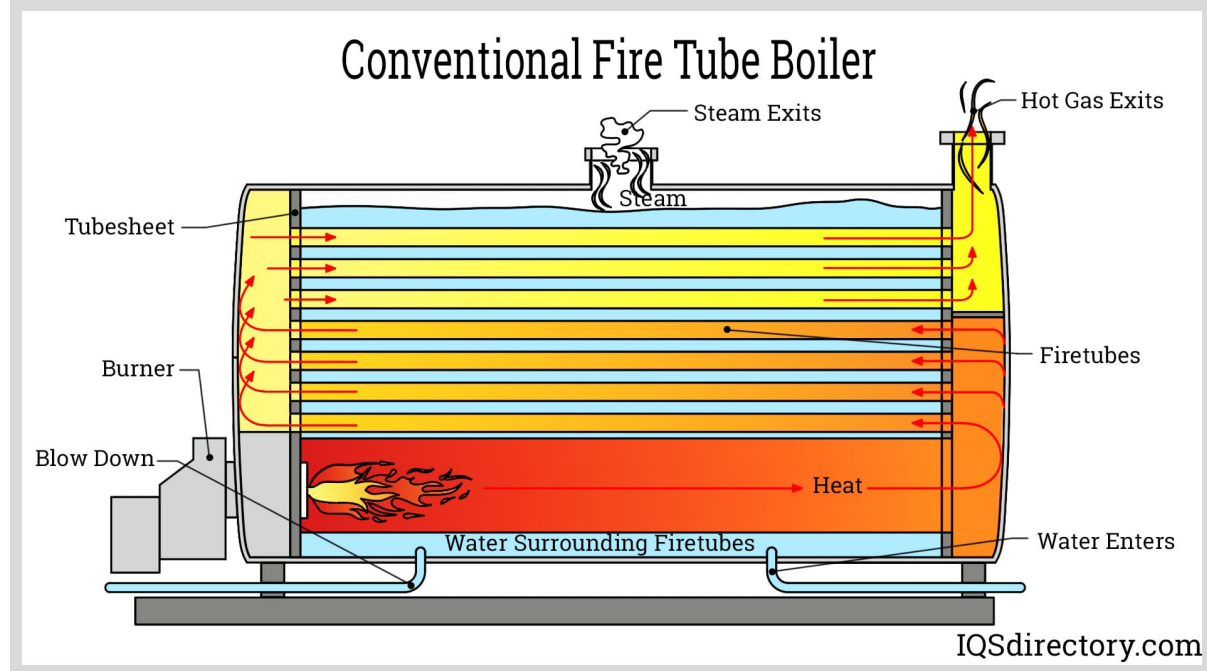


Figure 3.3: Detailed cross-section of the simulated boiler, showing drum, furnace, tube banks and reversal chambers (reproduced from [5]).

Drum

The boiler drum is modelled as a single horizontal cylindrical vessel without internal separators or circulation devices. It provides saturated liquid and vapour at drum pressure.

The inner diameter of the drum is $D_{i,\text{drum}} = 4.5 \text{ m}$ and the total length is $L_{\text{drum}} = 5.0 \text{ m}$

The drum wall is made of carbon steel with a uniform thickness of $t_{\text{drum}} = 0.05 \text{ m}$ and thermal conductivity $k_{\text{drum}} = 40 \text{ W m}^{-1}\text{K}^{-1}$

A fouling layer of thickness 0.1 mm and conductivity $0.2 \text{ W m}^{-1}\text{K}^{-1}$ is applied on the inner surface.

Pool boiling stages

All five pressure part stages located inside the drum are modelled under pool boiling conditions. These stages represent the furnace and convective passes before the economizer. Internal flow is one dimensional while external boiling occurs at drum saturation conditions.

All stages use steel walls with thermal conductivity $k_{\text{wall}} = 50 \text{ W m}^{-1}\text{K}^{-1}$, with internal roughness $\zeta_{\text{gas}} = 50 \mu\text{m}$, and outer roughness $\zeta_{\text{water}} = 20 \mu\text{m}$, while surface emissivity is 0.80.

Fouling resistance is included via a uniform fouling layer of thickness 0.1 mm and conductivity $0.2 \text{ W m}^{-1}\text{K}^{-1}$.

The main geometric parameters of the pool boiling stages are summarized in Table~3.1.

Table 3.1: Pool boiling pressure part geometry

Element Kind	D_i [m]	L [m]	Tube no.	Wall thickness [mm]	Roughness [μm]
HX1	single tube	1.40	5.276	1	20
HX2	reversal chamber	1.60	0.80	1	20
HX3	tube bank	0.076	4.975	118	2.9
HX4	reversal chamber	1.60	0.80	1	20
HX5	tube bank	0.076	5.620	100	2.9

The tube banks HX3 and HX5 are staggered arrangements with six tube rows. The transverse and longitudinal pitches are both $S_T = S_L = 0.11 \text{ m}$, respectively. Reversal chambers HX2 and HX4 include curvature effects through a bend radius of 0.8 m

Economizer

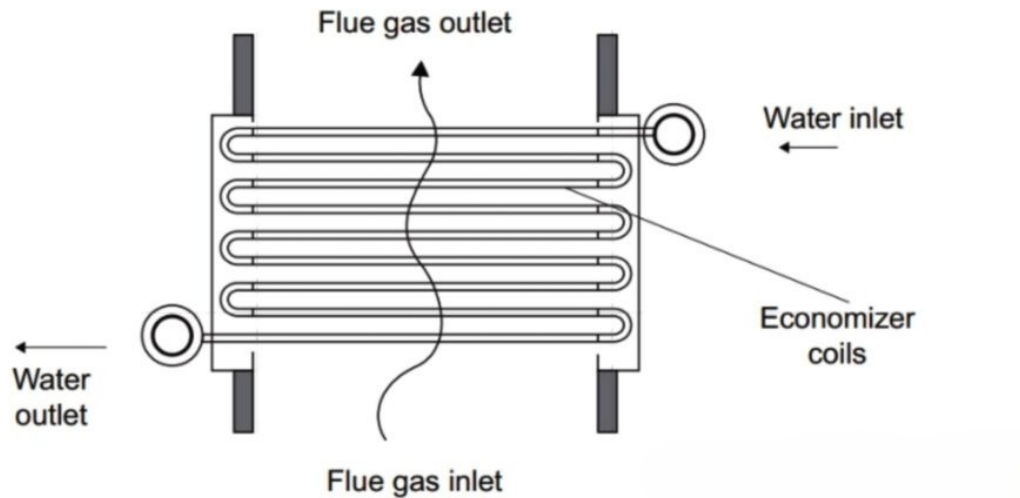


Figure 3.4: Cross-section of the economizer tube bundle HX_6 , showing gas-side cross-flow and water-side internal flow (reproduced from [6]).

The economizer is modelled as a shell and tube heat exchanger operating under single phase conditions on both sides. It is located downstream of the final pool boiling stage.

Flue gas flows on the shell side through a cylindrical duct of inner diameter $D_{\text{shell}} = 0.95 \text{ m}$. The tube side consists of 120 tubes of inner diameter $D_{i,\text{eco}} = 0.0250 \text{ m}$ with a tube length of $L_{\text{tube}} = 80 \text{ m}$.

The tube bundle is arranged in a staggered configuration. Transverse and longitudinal pitches are $S_T = 0.075 \text{ m}$ and $S_L = 0.08 \text{ m}$ respectively. Baffle spacing is 0.15 m with a baffle cut of 0.25 .

The economizer tubes are made of steel with wall thickness $t_{\text{eco}} = 2.6 \text{ mm}$ and thermal conductivity $k_{\text{eco}} = 50 \text{ W m}^{-1}\text{K}^{-1}$. Inner surface roughness is $20 \mu\text{m}$ and outer surface roughness is $50 \mu\text{m}$.

3.3 Assumptions and limitations

1. Combustion and flue gas

- Ideal complete combustion, with fixed excess air,
- Adiabatic flame temperature from equilibrium chemistry, using NASA polynomials.
- Ideal gas mixture $p = \rho RT$, with transport properties $\mu(T)$ $k(T)$ $c_p(T)$ from polynomial data.
- Steady state boiler operation, with fixed fuel air and feedwater.
- Boiler efficiency computed on HHV or LHV basis, using standard energy balance equations.

2. Heat transfer

- One dimensional steady heat transfer per stage.
- Uniform wall conductivity and thickness, radial conduction only.
- Gas side HTC from standard correlations properties **vary** with temperature pressure and composition.
- Gas radiation via band averaged grey model for CO_2 and H_2O , no spectral resolution, and no soot formation.
- Water side HTC uses IAPWS-IF97 properties, homogenized two phase model.
- Drum at fixed pressure, and perfect steam water separation (no carryover).

3. Hydraulic and thermal performance

- 1D, steady, single phase flow.
- Constant mass flow along each stage.
- Compressibility effects appear only through property variations $\rho(T, P)$ and $\mu(T, P)$ in Re and $\rho V^2/2$.

Chapter 4

Combustion Model

Determine combustion conditions inside the furnace (1st pass), resulting in a fully burnt flue gas stream, entering the heat transfer model at adiabatic temperature.

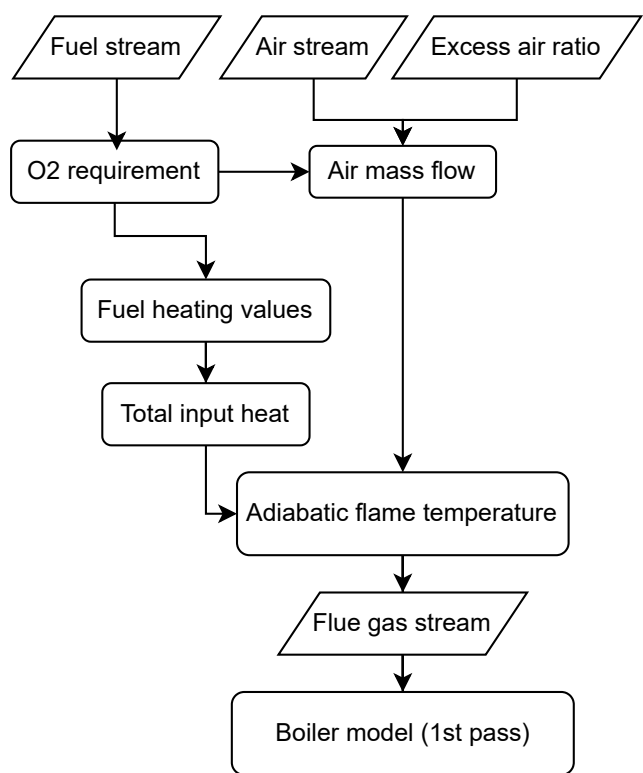


Figure 4.1: Combustion flow

4.1 Fuel and Air

4.1.1 Fuel Stream

The boiler is fired with a natural-gas-type fuel defined in the simulation input (config/fuel.yaml).

The fuel is supplied at $300K$ and $1.013 \times 10^5 Pa$ with a mass flow rate of $0.1kg/s$. Its composition is specified by user on a mass fraction.

Table 4.1: Fuel composition in mass fractions. [3]

Component	Formula	Mass fraction $w_i [-]$
Methane	CH_4	0.8548
Ethane	C_2H_6	0.0622
Propane	C_3H_8	0.0207
n-Butane	C_4H_{10}	0.00518
Hydrogen sulfide	H_2S	0.000104
Nitrogen	N_2	0.0414
Carbon dioxide	CO_2	0.0155
Water vapour	H_2O	0.00
Argon	Ar	0.00

The mass fractions sum to 1.0 by definition. The mole fractions x_i are obtained from

$$x_i = \frac{\frac{w_i}{M_i}}{\sum_j \frac{w_j}{M_j}} \quad (4.1)$$

which is provided by the function `to_mol` in `combustion/mass_mole.py`, where M_i is the molar mass of species i from `molar_masses` in `common/constants.py`.

4.1.2 Air Stream

Combustion air is represented as a separate `GasStream` object, analogous to the fuel stream, with:

- temperature $T_{air} = 300 K$,
- pressure $P_{air} = 1.013 \times 10^5 Pa$,
- mass flow rate determined internally from the specified excess air ratio λ ,
- composition:

Table 4.2: Air composition in mass fractions. [7]

Component	Formula	Mass fraction w_i [-]
Oxygen	O ₂	0.233
Nitrogen	N ₂	0.755
Argon	Ar	0.013
Carbon dioxide	CO ₂	0.00006

The mass fractions satisfy $\sum_i w_i = 1$ and are converted internally to mole fractions whenever stoichiometric or thermophysical properties are required.

4.1.3 Stoichiometric Oxygen requirement

Evaluated the stoichiometric oxygen requirement via `stoich_O2_required_per_mol_fuel` in `combustion/flue.py`. The algorithm is:

1. Use per mole of species stoichiometric O₂ factors $\nu_{O_{2,i}}$ from `o2_per_mol` in `common/constants.py`:

Table 4.3: Combustion reactions and stoichiometric factors

Species	Global reaction (complete combustion)	$\nu_{O_{2,i}}$ [mol O ₂ / mol species]
CH ₄	CH ₄ + 2 O ₂ → CO ₂ + 2 H ₂ O	2.0
C ₂ H ₆	C ₂ H ₆ + 3.5 O ₂ → 2 CO ₂ + 3 H ₂ O	3.5
C ₃ H ₈	C ₃ H ₈ + 5 O ₂ → 3 CO ₂ + 4 H ₂ O	5.0
C ₄ H ₁₀	C ₄ H ₁₀ + 6.5 O ₂ → 4 CO ₂ + 5 H ₂ O	6.5
H ₂ S	H ₂ S + 1 O ₂ → SO ₂ + H ₂ O	1.0
N ₂ , CO ₂ , H ₂ O	Inert/fully oxidized → no additional O ₂	0.0

2. Compute the stoichiometric O₂ requirement per mole of fuel mixture as

$$\nu_{O_2, \text{stoich}} = \sum_i x_i \nu_{O_2,i} \quad (4.2)$$

Using the mole fractions from Section 4.1 for the present fuel:

3. For later hydraulic and performance interpretation, it is also useful to express this on a mass basis.

For 1 kg of fuel, the total fuel moles are

$$n_{\text{fuel, total}} = \sum_i \frac{w_i}{M_i} \quad (4.3)$$

Thus the stoichiometric O₂ requirement per unit fuel mass is

$$n_{O_2,\text{stoich}}^{(m)} = \nu_{O_2,\text{stoich}} n_{\text{fuel},\text{total}} \quad (4.4)$$

Converting to mass of O₂ per kg of fuel:

$$\dot{m}_{O_2,\text{stoich}} = n_{O_2,\text{stoich}}^{(m)} M_{O_2} \quad (4.5)$$

4.1.4 Air-fuel ratio and excess air λ

The simulation specifies an excess air ratio $\lambda = 1.1$ in config/operation.yaml. This value enters the calculation through air_flow_rates(air, fuel, excess) in combustion/flue.py.

Actual O₂ supplied

Using:

$$\dot{n}_{O_2,\text{actual}} = \lambda \dot{n}_{O_2,\text{stoich}} = \lambda \nu_{O_2,\text{stoich}} \dot{n}_{\text{fuel}} \quad (4.6)$$

Air required

Air O₂ mole fraction (from air.yaml): $x_{O_2,\text{air}}$

Air moral flow, given by air_flow_rates():

$$\dot{n}_{\text{air}} = \frac{\dot{n}_{O_2,\text{actual}}}{x_{O_2,\text{air}}} \quad (4.7)$$

The air molar mass (mixture weighted) is:

$$M_{\text{air}} = \sum_i x_i M_i \quad (4.8)$$

Therefore the air mass flow rate:

$$\dot{m}_{\text{air}} = \dot{n}_{\text{air}} M_{\text{air}} \quad (4.9)$$

Air-fuel ratio

Mass based air fuel ratio:

$$\text{AFR} = \frac{\dot{m}_{\text{air}}}{\dot{m}_f} \quad (4.10)$$

4.2 Heating values and firing rate

The fuel lower and higher heating values, and the corresponding firing rate, are evaluated in `combustion/heat.py` by the function `compute_LHV_HHV(fuel, air)` and then used by `total_input_heat()`.

4.2.1 HHV and LHV

For each fuel species, complete combustion is considered:

- $\text{CH}_4 + 2 \text{O}_2 \rightarrow \text{CO}_2 + 2 \text{H}_2\text{O}$
- $\text{C}_2\text{H}_6 + 3.5 \text{O}_2 \rightarrow 2 \text{CO}_2 + 3 \text{H}_2\text{O}$

The implementation also supports heavier hydrocarbons (C_3H_8 , C_4H_{10}) and sulphur species (H_2S), which are handled using stoichiometric oxygen requirements.

Builds complete-combustion products assuming all water remains in the vapour phase. The lower heating value (LHV) is obtained directly from the gas-phase products.

The higher heating value (HHV) is obtained by adding the latent heat of condensation of the water formed.

Latent heat of water

Obtain the latent heat of vaporization of water at the reference pressure $P_{\text{ref}} = 101,325 \text{ Pa}$ from the IAPWS-97 correlation:

```
latent_H2O = WaterProps.h_g(P_ref) - WaterProps.h_f(P_ref)
```

where:

- h_g is the saturated vapour enthalpy,
- h_f is the saturated liquid enthalpy.

Reference thermodynamic data

All reactant and product enthalpies are obtained from the Cantera thermodynamic database via the mechanism file `config/flue_cantera.yaml`.

Mixture molar enthalpies are evaluated at the reference state $T_{\text{ref}} = 298.15 \text{ K}$ and $P_{\text{ref}} = 101,325 \text{ Pa}$ using Cantera's species NASA polynomial fits.

Methodology

The mixture molar heating values are computed directly from the molar enthalpy difference between reactants and products at the reference state:

$$\text{LHV}_{\text{mol}} = h_{\text{react}}(T_{\text{ref}}, P_{\text{ref}}) - h_{\text{prod}}(T_{\text{ref}}, P_{\text{ref}}) \quad (4.11)$$

The higher heating value is then obtained as

$$\text{HHV}_{\text{mol}} = \text{LHV}_{\text{mol}} + n_{\text{H}_2\text{O}} (h_g - h_f) M_{\text{H}_2\text{O}} \quad (4.12)$$

After obtaining the mixture molar heating values, conversion to mass basis uses

$$\text{HHV}_{\text{mix}} = \frac{\text{HHV}_{\text{mol}}}{M_{\text{mix}}}, \quad \text{LHV}_{\text{mix}} = \frac{\text{LHV}_{\text{mol}}}{M_{\text{mix}}}, \quad (4.13)$$

The firing rate corresponding to a fuel mass flow \dot{m}_f then follows directly:

$$P_{\text{HHV}} = \dot{m}_f \text{HHV}_{\text{mix}}, \quad P_{\text{LHV}} = \dot{m}_f \text{LHV}_{\text{mix}}. \quad (4.14)$$

4.2.2 Total heat input

The function `total_input_heat()` combines chemical and sensible contributions: where `sensible_heat()` uses:

$$Q_{\text{sens}} = \dot{m} [h(T, P, Y) - h(T_{\text{ref}}, P, Y)] \quad (4.15)$$

Both fuel and air enter at 300 K, while the reference is 298.15 K; the resulting sensible contributions are very small compared with the chemical term P_{LHV} (on the order of tens of kW versus tens of MW). Therefore:

$$Q_{\text{in}} = P_{\text{LHV}} + Q_{\text{sens,fuel}} + Q_{\text{sens,air}} \approx P_{\text{LHV}} \quad (4.16)$$

4.3 Flame and flue gas

The combustion model must provide two closely related but conceptually distinct outputs:

1. The adiabatic flame temperature T_{ad} and equilibrium combustion state, which define the thermodynamic upper limit of the combustion process.
2. A practical flue-gas stream to be used as the hot-side working fluid in the boiler heat-transfer and pressure-drop calculations.

These two objectives place conflicting requirements on the combustion model. Accurate prediction of T_{ad} requires a full chemical-equilibrium treatment including high-temperature dissociation. In contrast, boiler heat-transfer and hydraulics require a chemically frozen reduced product set with stable thermophysical properties.

For this reason, the model deliberately computes two distinct flue-gas representations from the same reactant energy balance:

- an equilibrium flue gas used solely to determine T_{ad} and equilibrium composition, and
- a fully burnt boiler flue gas used as the working fluid throughout the boiler model.

Both streams are derived from the same inlet conditions and satisfy the same adiabatic, constant-pressure energy balance, but they differ in their chemical treatment and intended use.

4.3.1 Methodology

Fuel and air are assumed to mix perfectly and react adiabatically at constant pressure P , equal to the inlet pressure. Heat losses and shaft work are neglected.

The total inlet enthalpy rate of the unmixed reactants is

$$\dot{H}_{\text{react}} = \dot{m}_{\text{air}} h_{\text{air}}(T_{\text{air}}, P, \mathbf{x}_{\text{air}}) + \dot{m}_{\text{fuel}} h_{\text{fuel}}(T_{\text{fuel}}, P, \mathbf{x}_{\text{fuel}}) \quad (4.17)$$

with total mass flow

$$\dot{m}_{\text{tot}} = \dot{m}_{\text{air}} + \dot{m}_{\text{fuel}}. \quad (4.18)$$

The target specific enthalpy of the reacting mixture is therefore

$$h_{\text{target}} = \frac{\dot{H}_{\text{react}}}{\dot{m}_{\text{tot}}}. \quad (4.19)$$

The overall reactant composition is constructed from the molar flow rates of each species in the fuel and air streams.

Reactant species molar flow rates are obtained by converting inlet mass fractions to mole fractions and scaling by the corresponding total molar flow rates:

$$\dot{n}_i^{(\text{air})}, \quad \dot{n}_i^{(\text{fuel})}. \quad (4.20)$$

The total molar flow rate of species i is

$$\dot{n}_i = \dot{n}_i^{(\text{air})} + \dot{n}_i^{(\text{fuel})}, \quad (4.21)$$

and the overall reactant mole fractions are

$$X_{i,\text{react}} = \frac{\dot{n}_i}{\sum_j \dot{n}_j}. \quad (4.22)$$

This reactant mixture, together with h_{target} and pressure P , defines the common thermodynamic basis for both flue-gas representations described below.

4.3.2 Equilibrium flame state and adiabatic flame temperature

The equilibrium flame state is computed using Cantera by enforcing chemical equilibrium at constant enthalpy and pressure:

$$\begin{aligned} h_{\text{products}}(T_{\text{ad}}, P, \mathbf{X}_{\text{eq}}) &= h_{\text{target}}, \\ P_{\text{out}} &= P, \end{aligned} \quad (4.23)$$

where \mathbf{X}_{eq} satisfies chemical equilibrium at (T_{ad}, P) .

The reacting mixture is initialized at $T = 300$ K, pressure P , and composition $\mathbf{X}_{\text{react}}$, and Cantera's HP equilibrium solver is used to determine the equilibrium temperature and species composition.

The resulting equilibrium flue gas:

- includes all species permitted by the chemical mechanism, including dissociation products,
- defines the adiabatic flame temperature T_{ad} ,
- is used exclusively for combustion diagnostics and performance assessment.

This stream is not used in downstream boiler calculations.

4.3.3 Boiler flue gas

For boiler heat-transfer and pressure-drop calculations, a second flue-gas stream is constructed assuming complete combustion without dissociation.

Complete oxidation is implemented explicitly for a fixed fuel species set (CH_4 , C_2H_6 , C_3H_8 , C_4H_{10} , H_2S), accounting for any CO_2 , H_2O , N_2 , and Ar present in the inlet streams, and assuming excess-air operation ($\lambda \geq 1$). The resulting product set is limited to stable species such as CO_2 , H_2O , N_2 , O_2 , Ar, and SO_2 .

The boiler flue-gas temperature T_{flue} is obtained from an adiabatic, constant-pressure energy balance:

$$h_{\text{products}}(T_{\text{flue}}, P, \mathbf{Y}_{\text{burnt}}) = h_{\text{target}}. \quad (4.24)$$

This fully burnt, chemically frozen flue gas:

- satisfies the same overall energy balance as the equilibrium flame state,
- has a reduced, stable species set suitable for property evaluation,
- is used as the hot-side working fluid in all boiler heat-transfer and pressure-drop calculations.

Chapter 5

Heat Transfer Model

This model simulates heat transfer from hot flue gas to the water/steam mixture in the drum, flue gas entering first pass, is specified by the results of the combustion model as fully burnt gas at adiabatic temperature with known mass flow rate, and water entering the economizer, specified by user at 10bar pressure and 105°C temperature with the mass flow to be calculated iteratively until convergence of water in and steam produced.

5.1 Fundamental heat balance equations

The boiler is modelled as a one dimensional counter current heat exchanger composed of six stages (HX_1 – HX_5). Heat transfer is resolved along the gas flow direction x , while water flows in the opposite direction. Each stage is discretized into segments of length dx ; all local quantities are defined per unit length.

- Notation (per segment)
- x – axial coordinate along the gas flow [m]
- dx – marching step in x [m]
- \dot{m}_g, \dot{m}_w – gas and water mass flow rates [kg/s]
- $T_g(x), T_w(x)$ – bulk gas and water temperatures [K]
- $T_{gw}(x), T_{ww}(x)$ – gas-side and water-side wall temperatures [K]
- $h_g(x), h_w(x)$ – total gas-side and water-side heat-transfer coefficients [$W/m^2 \cdot K$]
- P_g, P_w – gas-side and water-side wetted perimeters [m]
- $q'(x)$ – linear heat flux (heat per unit length) [W/m]
- $UA'(x)$ – overall conductance per unit length [$W/K/m$]

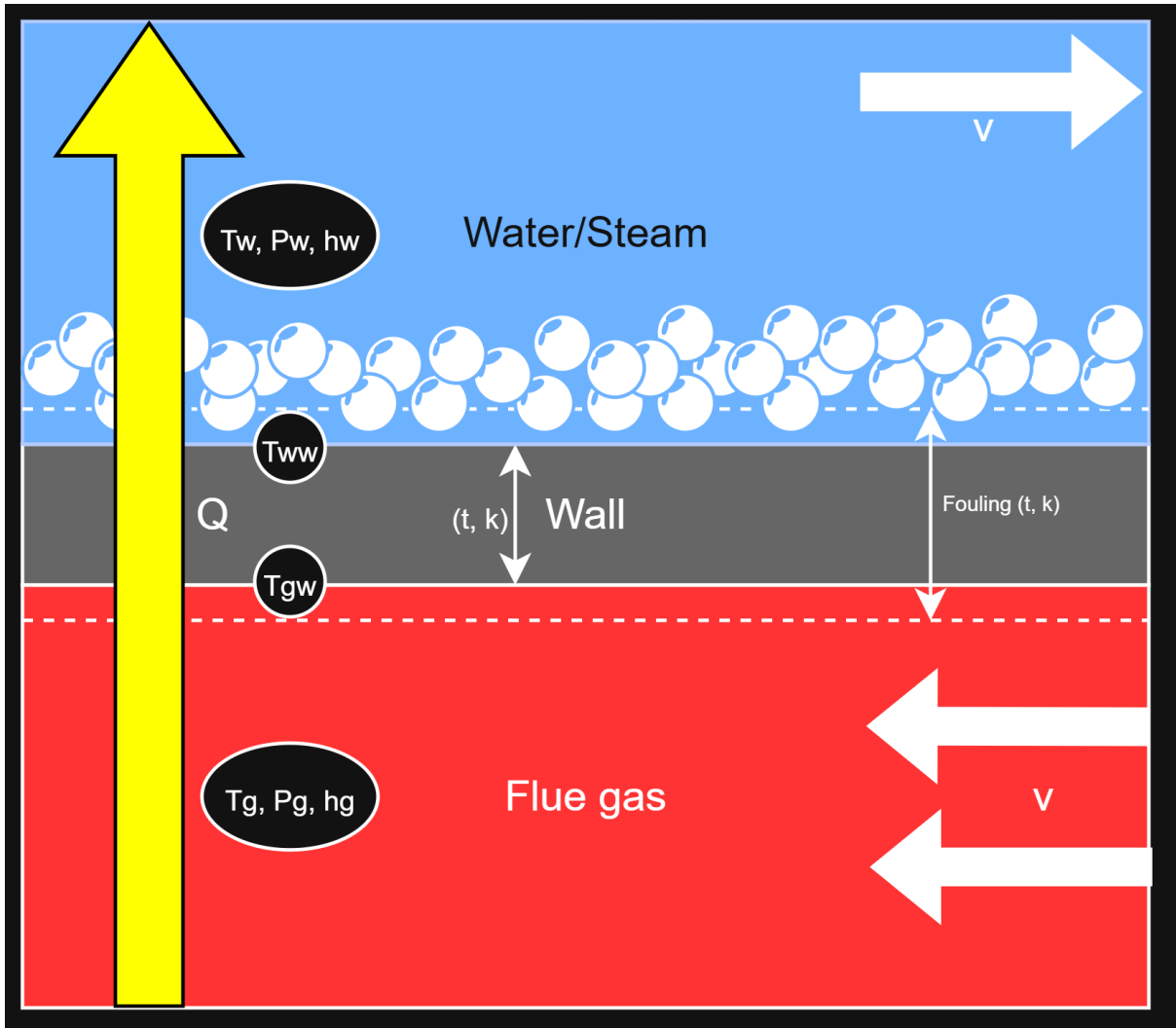


Figure 5.1: Cross section of heat transfer network from gas to water/steam

5.2 Local energy balance

For each differential segment of length dx , the model enforces a one dimensional steady state energy balance between the gas, the water and the tube wall:

- Heat transferred across the wall:

$$q'(x) = UA'(x) [T_g(x) - T_w(x)] \quad (5.1)$$

- Relation to the segment duty:

$$dQ(x) = q'(x) dx \quad (5.2)$$

- Gas stream:

$$dQ(x) = -\dot{m}_g dh_g(x) \Rightarrow \frac{dh_g}{dx} = -\frac{q'(x)}{\dot{m}_g} \quad (5.3)$$

- Water stream:

$$dQ(x) = +\dot{m}_w dh_w(x) \Rightarrow \frac{dh_w}{dx} = +\frac{q'(x)}{\dot{m}_w} \quad (5.4)$$

In the numerical implementation these equations are applied in finite difference form over each marching step:

$$Q_{\text{step}} = q'(x) \Delta x \quad (5.5)$$

$$\Delta h_g = -\frac{Q_{\text{step}}}{\dot{m}_g}, \quad \Delta h_w = +\frac{Q_{\text{step}}}{\dot{m}_w} \quad (5.6)$$

5.3 Overall conductance and resistance network

The overall conductance per unit length $UA'(x)$ is obtained from a radial series of thermal resistances per unit length:

- Gas side convection:

$$R'_g = \frac{1}{h_g(x) P_g} \quad (5.7)$$

- Gas side fouling:

$$R'_{fg} = R'_{fi}(P_g) \quad (\text{from specified fouling thickness and conductivity}) \quad (5.8)$$

- Tube wall:

$$R'_w = \frac{\ln(D_o/D_i)}{2\pi k_w} \quad (5.9)$$

- Water side fouling:

$$R'_{fc} = R'_{fo}(P_w) \quad (5.10)$$

- Water side convection:

$$R'_c = \frac{1}{h_w(x) P_w} \quad (5.11)$$

where D_i and D_o are the tube inner and outer diameters and k_w is the tube wall thermal conductivity. Combining these contributions:

$$\frac{1}{UA'(x)} = R'_g + R'_{fg} + R'_w + R'_{fc} + R'_c \quad (5.12)$$

or equivalently,

$$UA'(x) = \left[\frac{1}{h_g P_g} + R'_{fg} + R'_w + R'_{fc} + \frac{1}{h_w P_w} \right]^{-1} \quad (5.13)$$

The linear heat flux then follows directly:

$$q'(x) = UA'(x) [T_g(x) - T_w(x)] \quad (5.14)$$

5.4 Wall temperature update and thermal convergence

The tube wall temperatures on the gas and water sides, T_{gw} and T_{ww} , are updated using a two node wall model in each marching step.

Given $q'(x)$, the wall side energy balances yield:

$$T_{gw} = T_g - \frac{q'}{h_{g,\text{tot}}} \quad (5.15)$$

$$T_{ww} = T_w + \frac{q'}{h_w} \quad (5.16)$$

The wall conduction temperature drop is:

$$\Delta T_{\text{wall}} = T_{gw} - T_{ww} \quad (5.17)$$

which is also equal to:

$$\Delta T_{\text{wall}} = q' [R'_{fg} + R'_w + R'_{fc}] \quad (5.18)$$

A consistency check is applied; if the implied wall temperature difference from conduction differs from the one implied by convection, the marching solver iterates the HTC evaluation once with relaxed updates (default under-relaxation factor 0.35).

In the actual implementation this consistency check is performed by iterating on T_{gw} , T_{ww} , and q' using the full resistance network (gas convection, gas fouling, wall, water fouling, water convection), with an under-relaxation factor applied to both wall temperatures and the linear heat flux.

If temperature overshoot (negative film coefficient, reversed driving force) is detected within a step, the step is automatically halved and recomputed.

5.5 Stage and boiler level duties

For a stage of length L_j , the stage heat duty and stage level conductance are obtained by integrating the local quantities along x :

$$Q_{\text{stage},j} = \int_0^{L_j} q'(x) \, dx \approx \sum_i q'_i \Delta x_i \quad (5.19)$$

$$(UA)_j = \int_0^{L_j} UA'(x) \, dx \approx \sum_i UA'_i \Delta x_i \quad (5.20)$$

The total useful boiler duty is the sum of all stage duties:

$$Q_{\text{useful}} = \sum_{j=1}^6 Q_{\text{stage},j} \quad (5.21)$$

These integrated quantities are later used in the performance and efficiency evaluation (Section 7) and for constructing stage-wise summary tables.

5.6 Gas side

Gas side heat transfer is computed with geometry aware correlations based on local gas properties from Cantera (`GasProps`) and stage specific geometry from the `GeometryBuilder`. For each marching step, the total gas side HTC is split into a convective and a radiative contribution:

$$h_{g,\text{tot}} = h_{g,\text{conv}} + h_{g,\text{rad}} \quad (5.22)$$

The implementation uses the helper `gas_htc_parts(g, spec, T_{gw})`, which returns $(h_{g,\text{conv}}, h_{g,\text{rad}})$ in $\text{W/m}^2\cdot\text{K}$, and then sums them in `gas_htc`.

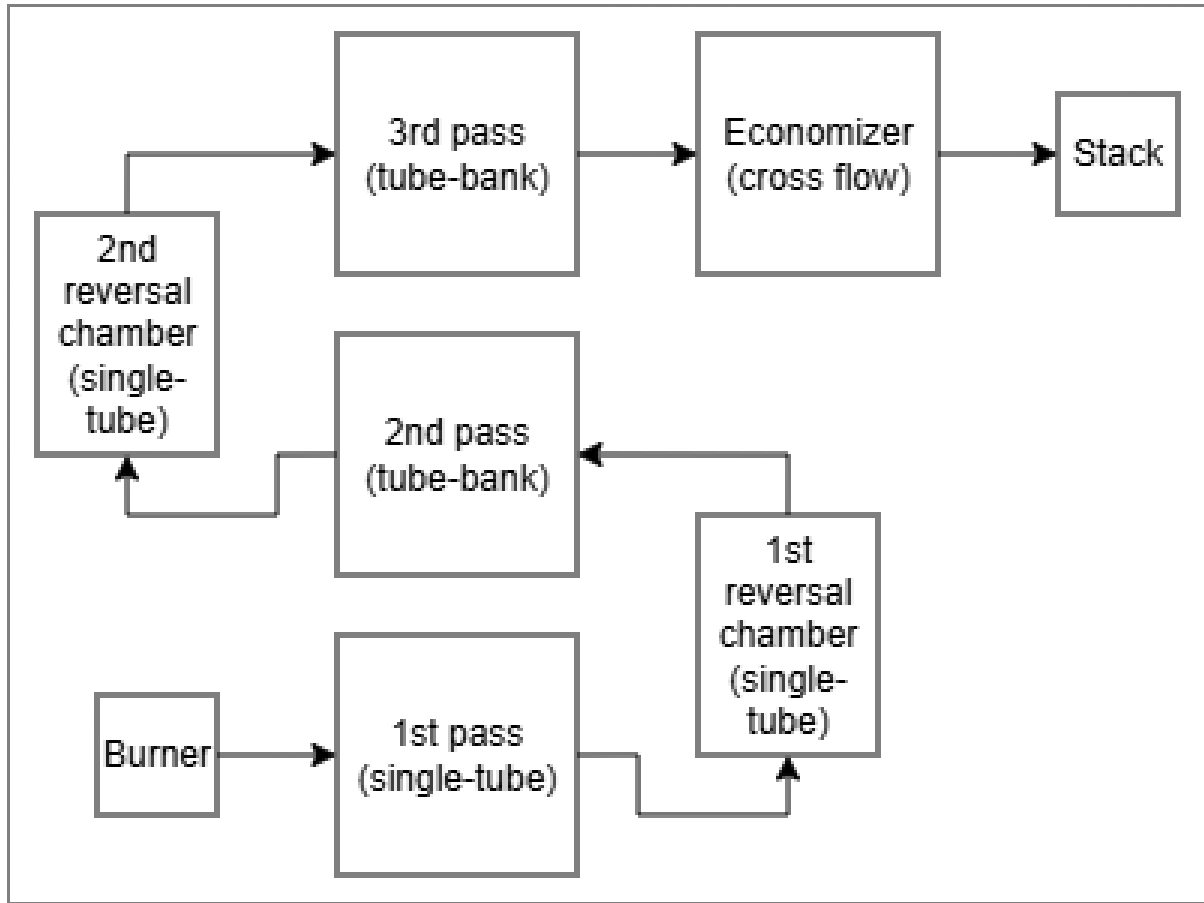


Figure 5.2: Path of flue gas through the 6 stages

5.6.1 Single tube and reversal chamber

Stages of kind `single_tube` and `reversal_chamber`, corresponding to furnace (first pass), and both reversal chambers, are treated as internal forced convection in a circular duct. The characteristic quantities are:

- Diameter: D (supplied by `stages.yaml`)
- Length: L (supplied by `stages.yaml`)
- Flow area: $A = \frac{1}{4} \pi D^2$ (calculated by geometry builder)
- Velocity:

$$V = \frac{\dot{m}_g}{\rho_g A} \quad (5.23)$$

- Reynolds and Prandtl numbers:

$$\text{Re} = \frac{\rho_g V D}{\mu_g}, \quad \text{Pr} = \frac{c_{p,g} \mu_g}{k_g} \quad (5.24)$$

Local gas properties $\rho_g, \mu_g, k_g, c_{p,g}$ are obtained from the Cantera mixture via the functions defined in `common\props.py`, at the local gas temperature and pressure. [8]

Laminar/developing flow (Graetz-type)

For $\text{Re} < 2300$, uses a Graetz correlation for thermally developing laminar flow:

$$Gz = \text{Re} \Pr \frac{D}{L} \quad (5.25)$$

$$\text{Nu} = 3.66 + \frac{0.0668 Gz}{1 + 0.04 Gz^{2/3}} \quad (5.26)$$

[2]

Turbulent flow (Gnielinski with Petukhov friction factor)

For $\text{Re} \geq 2300$, the Gnielinski correlation is applied with a Petukhov friction factor:

$$f = (0.79 \ln \text{Re} - 1.64)^{-2} \quad (5.27)$$

[10]

$$\text{Nu} = \frac{\frac{f}{8}(\text{Re} - 1000) \Pr}{1 + 12.7 \sqrt{\frac{f}{8}} (\Pr^{2/3} - 1)} \quad (5.28)$$

[2] The local convective heat-transfer coefficient is then:

$$h_{g,\text{conv}} = \frac{\text{Nu} k_g}{D} \quad (5.29)$$

[2]

This same internal correlation is used for `single_tube`, `reversal_chamber` and `tube_bank` gas-side flow (see below).

5.6.2 Tube bank

Stages `tube_bank` correspond to tube bundles inside the shell, ie. first and second passes. In this model, the gas side is still treated as internal flow inside the tubes:

- Hot side (gas): inside tubes (inner diameter D_i), using the same internal forced convection model as in Section 5.2.1.

Thus the gas side convective HTC in tube-bank stages is:

$$h_{g,\text{conv}}^{(\text{HX3,5})} = \frac{\text{Nu}(\text{Re}, \Pr) k_g}{D_i} \quad (5.30)$$

with Nu given by the Graetz/Gnielinski formulation above, and Re , Pr computed from the local gas properties and tube hydraulic diameter.

5.6.3 Economizer

The economizer stage reverses the roles: gas flows outside the tubes in cross flow, while water flows inside. The gas side convection is then modelled as external cross flow over a tube bank.

Key geometry quantities (from GeometryBuilder for the economizer):

- Tube outer diameter: $D = D_o$
- Gas side cross flow area: $A_{\text{bulk}} = A_{\text{hot,flow}}$
- Optional maximum/mean velocity factor:

$$V_{\text{bulk}} = \frac{\dot{m}_g}{\rho_g A_{\text{bulk}}}, \quad V = u_{\max} V_{\text{bulk}} \quad (5.31)$$

where u_{\max} is calculated depending on the tube bank arrangement and spacing between tubes.

- Reynolds and Prandtl numbers:

$$\text{Re} = \frac{\rho_g V D}{\mu_g}, \quad \text{Pr} = \frac{c_{p,g} \mu_g}{k_g} \quad (5.32)$$

For "economiser" stages the primary correlation is a banded Zukauskas form for cross flow over tube banks:

$$\text{Nu} = C \text{Re}^m \text{Pr}^n \quad (5.33)$$

[2]

where the coefficients C, m are selected from standard bands as a function of Reynolds number and tube arrangement (inline vs staggered), and the exponent n is:

$$n = \begin{cases} 0.36, & \text{Pr} \leq 10 \\ 0.25, & \text{Pr} > 10 \end{cases} \quad (5.34)$$

If Re falls outside the tabulated bands, the model falls back to the Churchill–Bernstein correlation for cross flow over a single cylinder:

$$\text{Nu} = 0.3 + \frac{0.62 \text{Re}^{1/2} \text{Pr}^{1/3}}{\left[1 + (0.4/\text{Pr})^{2/3}\right]^{1/4}} \left[1 + \left(\frac{\text{Re}}{282000}\right)^{5/8}\right]^{4/5} \quad (5.35)$$

[2] The gas-side convective HTC in the economizer is then:

$$h_{g,\text{conv}}^{(\text{HX6})} = \frac{\text{Nu } k_g}{D_o} \quad (5.36)$$

[2]

5.6.4 Radiation model

Radiative heat transfer from the flue gas to the furnace surfaces is explicitly accounted for by a participating medium model for the H_2O/CO_2 mixture. The implementation follows a simplified Smith–Shen–Friedman style four gray model.

For each step, the gas emissivity is computed as:

1. Partial pressures of participating species:

$$p_{H_2O} = y_{H_2O} P, \quad p_{CO_2} = y_{CO_2} P \quad (5.37)$$

[9] where y_i are molar (or mass-fraction-equivalent) composition entries from the flue gas stream, and P is the local gas pressure.

2. Mean beam length:

$$L_b = \begin{cases} L_{\text{rad,override}}, & \text{if specified in the stage} \\ 0.9 D_{h,\text{gas}}, & \text{otherwise} \end{cases} \quad (5.38)$$

[9] with $D_{h,\text{gas}}$ the gas-side hydraulic diameter.

3. Effective optical thickness in each gray band:

$$p_{\text{ratio}} = \frac{p_{H_2O} + p_{CO_2}}{P_{\text{atm}}} \quad (5.39)$$

[9]

$$\tau_j = K_j \left(\frac{T}{1000 \text{ K}} \right)^{T_{\text{exp}}} p_{\text{ratio}} L_b \quad (5.40)$$

[9]

where K_j and weighting factors A_j are fixed band coefficients, T is the gas temperature, and T_{exp} is a temperature exponent (default 0.65, configurable per stage via `rad_Texp`).

4. Total gas emissivity:

$$\varepsilon_g = 1 - \sum_{j=1}^4 A_j \exp(-\tau_j) \quad (5.41)$$

[9] with ε_g constrained to $[0, 1]$.

A mean-film temperature is used for the linearized radiative HTC:

$$T_{\text{film}} = \frac{T_g + T_{gw}}{2} \quad (5.42)$$

$$h_{g,\text{rad}} = 4 \sigma F \varepsilon_g T_{\text{film}}^3 \quad (5.43)$$

[9]

where:

- σ is the Stefan–Boltzmann constant,
- F is an effective view factor (default 1.0 or stage-specific `rad_F`).

The gas-side total HTC reported and used in the resistance network is then:

$$h_{g,\text{tot}} = h_{g,\text{conv}} + h_{g,\text{rad}} \quad (5.44)$$

and the corresponding convective/radiative contributions to the linear heat flux are tracked via:

$$q'_{\text{conv}} = q' \frac{h_{g,\text{conv}}}{h_{g,\text{tot}}}, \quad q'_{\text{rad}} = q' - q'_{\text{conv}} \quad (5.45)$$

These diagnostics are later integrated on a per-stage basis to quantify the share of convective vs radiative heat transfer in each section of the boiler.

5.7 Water side

Water side heat transfer is computed with geometry dependent correlations using local water properties from IAPWS97 (`WaterProps`), with stage specific geometry from the `GeometryBuilder`. The solver always works with a single effective water side heat transfer coefficient $h_w(x)$ per marching step, which may represent:

- pure pool boiling at a saturated surface,
- a Chen type combination of forced convection and nucleate boiling, or
- single phase forced convection.

In the implementation this logic is encapsulated in `water_htc`, which returns (h_w) for each step.

5.7.1 General formulation and boiling treatment

The six stages of the boiler are divided, from the water-side point of view, into:

- $\text{HX}_1\text{--}\text{HX}_5$: pool-boiling stages
(`pool_boiling = true` in the stage specification)
- HX_6 : economizer stage
(`pool_boiling = false`)

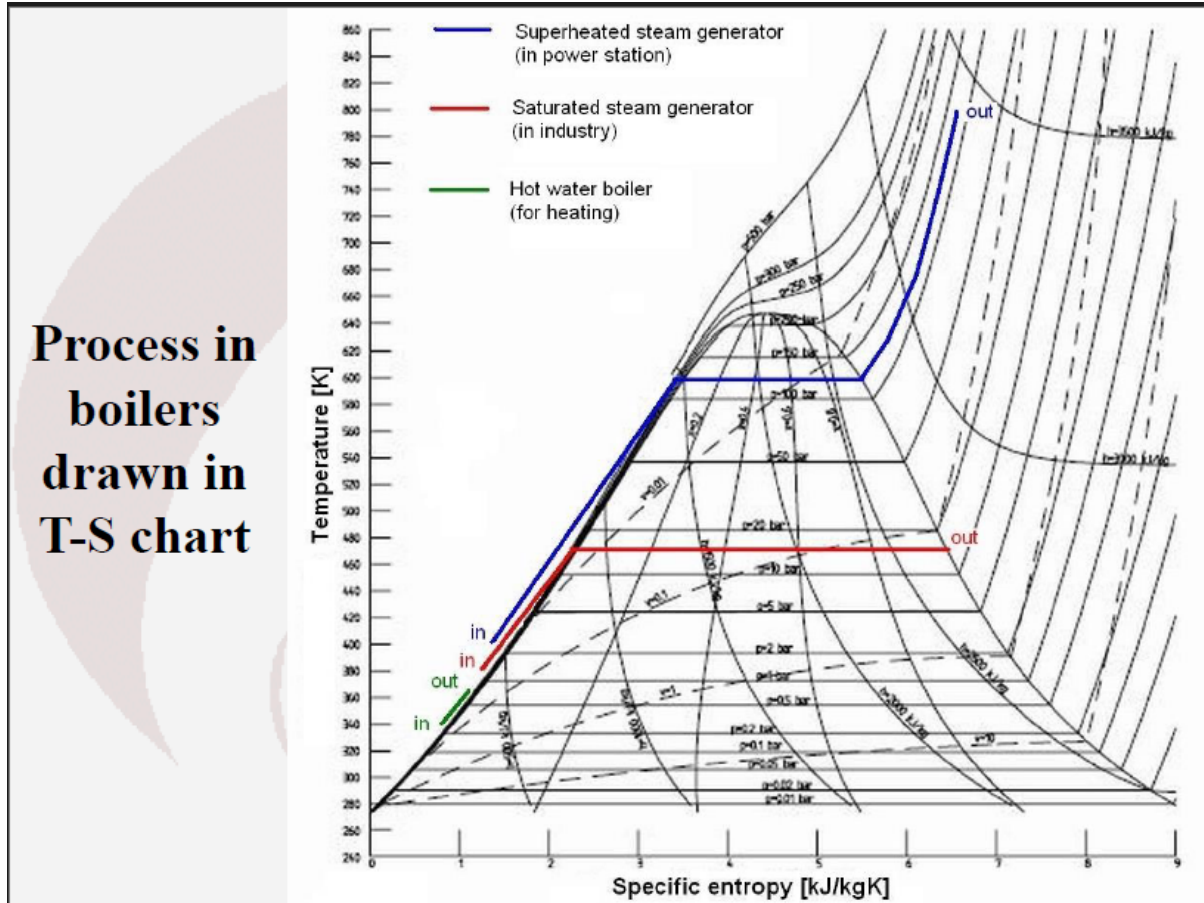


Figure 5.3: Temperature–entropy (T – s) representation of the feedwater heating and evaporation process across economiser and boiler at the operating pressure (reproduced from [4]).

The solver applies the following decision tree at each marching step:

1. Pool-boiling stages ($\text{HX}_1\text{--}\text{HX}_5$)

If the stage is flagged as `pool_boiling = true`, the bulk water temperature entering the wall-energy balance is fixed at the saturation temperature at the local pressure:

$$T_w = T_{\text{sat}}(p_w), \quad (5.46)$$

and the water-side HTC is computed from the Cooper pool boiling correlation for nucleate boiling correlation:

$$h_{\text{Cooper}} = 55 p_r^{0.12} R_p^{-0.55} M_w^{-0.5} (q'')^{0.67} \quad (5.47)$$

where

$$p_r = \frac{p}{p_{\text{crit}}} = \text{reduced pressure}, \quad R_p = \text{surface roughness } (\mu\text{m}), \quad q'' = \text{heat flux.} \quad (5.48)$$

[2]

This nucleate-boiling HTC is then used directly:

$$h_w = h_{w,\text{nb}}, \quad (5.49)$$

and the step is always marked as boiling in the post processing.

In other words, the main boiling surfaces of the boiler (furnace, passes, reversal chambers) are represented as heated surfaces in a saturated pool, with the HTC governed by the local heat flux and surface roughness rather than by a detailed prediction of liquid velocity. This matches the natural circulation character of these sections.

2. Non pool boiling stages (HX₆, economizer)

For stages with `pool_boiling = false`, the model can represent both single phase convection and flow boiling via a Chen type formulation.

a. Boiling detection

A helper determines whether the local state is boiling based on the bulk enthalpy h and, when needed, the wall temperature T_{wall} :

- if

$$h_f(p_w) \leq h \leq h_g(p_w) \quad (5.50)$$

the state is inside the saturation interval and is treated as two phase;

- if $h < h_f(p_w)$ (slightly subcooled liquid) but the wall superheat is sufficiently high,

$$T_{\text{wall}} > T_{\text{sat}}(p_w) + \Delta T_{\text{crit}}, \quad (5.51)$$

the state is also treated as boiling;

- otherwise the flow is treated as single-phase liquid.

Here h_f and h_g are saturated-liquid and saturated vapor enthalpies at the local pressure, obtained via IAPWS97.

b. Single-phase regime

If boiling is not detected, the water side HTC is purely convective:

$$h_w = h_{w,\text{conv}}, \quad (5.52)$$

with $h_{w,\text{conv}}$ obtained from a geometry dependent forced convection correlation (internal tube, external tube bank, or external single tube/bend) as detailed in Sections [5.7.2]–[5.7.4].

c. Flow boiling regime (Chen model)

When boiling is detected in a non pool boiling stage, the HTC is constructed as a Chen type superposition of:

- a liquid only convective term h_{lo} , and
- a nucleate-boiling term h_{nb} using the same Cooper correlation as in pool boiling.

The liquid only HTC is evaluated at the saturation temperature $T_{\text{sat}}(p)$ and using the appropriate geometry correlation:

$$h_{\text{lo}} = h_{\text{single-phase}}(T_{\text{sat}}(p), \text{geometry}), \quad (5.53)$$

while the nucleate-boiling term is

$$h_{\text{nb}} = h_{\text{Cooper}}(p, q''). \quad (5.54)$$

The Chen combination used in the code is:

$$h_w = F h_{\text{lo}} + S h_{\text{nb}}. \quad (5.55)$$

[2]

The convection enhancement factor F is based on a Martinelli type parameter X_{tt} ,

$$X_{tt} = \left(\frac{1-x}{x}\right)^{0.9} \left(\frac{\mu_l}{\mu_g}\right)^{0.1} \left(\frac{\rho_g}{\rho_l}\right)^{0.5}, \quad (5.56)$$

where x is the local vapor quality and $\rho_l, \rho_g, \mu_l, \mu_g$ are liquid/vapor densities and viscosities at saturation. A bounded form of the Chen factor is then used:

$$F = 1 + 0.12 X_{tt}^{-0.8}, \quad (5.57)$$

The suppression factor S modulating the nucleate boiling contribution is a function of mass flux and Reynolds number:

$$S = \frac{1}{1 + C \text{Re}_{\text{lo}}^\alpha}, \quad (5.58)$$

where Re_{lo} is a liquid only Reynolds number based on the mass flux

$$G = \frac{\dot{m}_w}{A_{\text{flow}}}, \quad (5.59)$$

and the liquid properties at saturation. In the implementation the constants and bounds are chosen such that S remains between about 0.1 and 1.0, reducing the nucleate boiling influence at very high mass flux (strong forced convection).

In the present thesis this Chen type flow boiling capability is only exercised in the economizer stage; the main boiling sections (HX_1 – HX_5) use the pure pool boiling representation above.

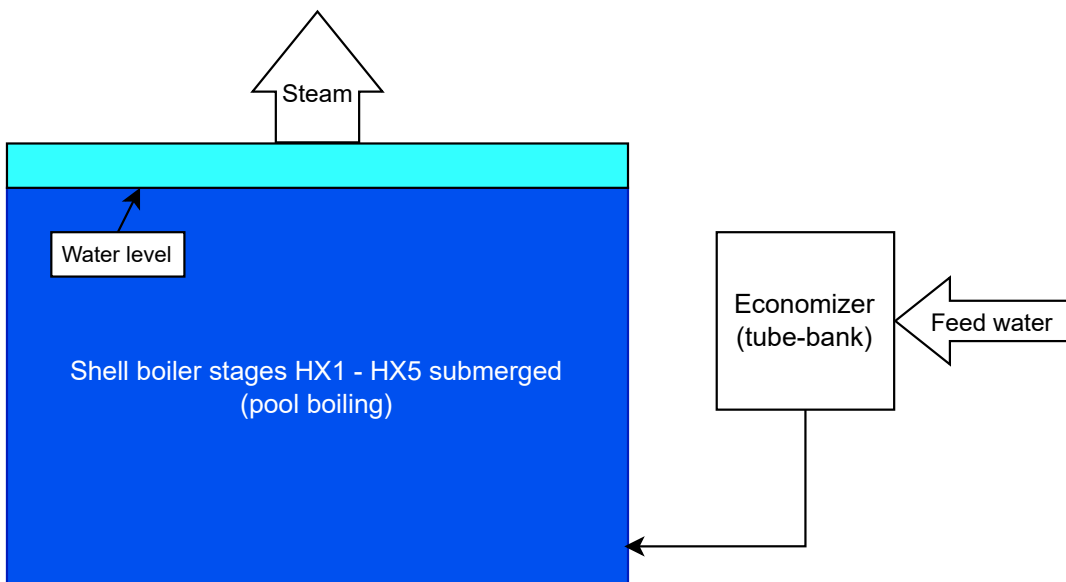


Figure 5.4: Path of water/steam through the 6 stages

5.7.2 Economizer

In the economizer stage (HX_6 , kind = "economiser"), water flows inside the tubes and is heated by the flue gas flowing externally in cross flow. This stage is the only one where `pool_boiling = false` and where the full single phase/Chen type boiling formulation is used.

Velocity and dimensionless groups

The relevant geometric quantities for the water side are:

- tube inner diameter: D_i ,
- tube length: L ,
- cold-side flow area: $A_{\text{cold,flow}}$.

The bulk water velocity, Reynolds and Prandtl numbers are:

$$V_w = \frac{\dot{m}_w}{\rho_w A_{\text{cold,flow}}}, \quad (5.60)$$

$$\text{Re}_w = \frac{\rho_w V_w D_i}{\mu_w}, \quad \text{Pr}_w = \frac{c_{p,w} \mu_w}{k_w}, \quad (5.61)$$

with $\rho_w, \mu_w, k_w, c_{p,w}$ evaluated from IAPWS97 at the film temperature. [14]

Single phase internal flow correlation

When no boiling is detected in the economizer, the Nusselt number is computed using a Gnielinski type internal flow correlation with a viscosity ratio correction:

- Laminar / developing regime ($\text{Re}_w < 2300$): a Graetz type form is used

$$\text{Gz}_w = \text{Re}_w \text{Pr}_w \frac{D_i}{L}, \quad (5.62)$$

$$\text{Nu}_w = 3.66 + \frac{0.0668 \text{Gz}_w}{1 + 0.04 \text{Gz}_w^{2/3}}. \quad (5.63)$$

- Turbulent regime ($\text{Re}_w \geq 2300$): Gnielinski correlation with friction factor

$$f_w = (0.79 \ln \text{Re}_w - 1.64)^{-2}, \quad (5.64)$$

[10]

$$\text{Nu}_w = \frac{\frac{f_w}{8} (\text{Re}_w - 1000) \text{Pr}_w}{1 + 12.7 \sqrt{\frac{f_w}{8}} (\text{Pr}_w^{2/3} - 1)}, \quad (5.65)$$

[2] scaled by a viscosity-ratio correction:

$$\text{Nu}_w \leftarrow \text{Nu}_w \left(\frac{\mu_b}{\mu_w} \right)^{0.11}, \quad (5.66)$$

where μ_b is evaluated at the bulk temperature and μ_w at the wall temperature.

The single phase water side HTC in the economizer is then:

$$h_{w,\text{conv}}^{(\text{HX6})} = \frac{\text{Nu}_w k_w}{D_i}. \quad (5.67)$$

[2]

Flow boiling in the economizer

If boiling is detected in the economizer (according to the criteria in the general formulation), the same geometry and mass flux information are used to form the liquid only HTC h_{lo} and the Cooper nucleate boiling HTC h_{nb} . The total water side HTC is then:

$$h_w = F h_{lo} + S h_{nb}, \quad (5.68)$$

with F and S given by the Chen type relations described above, using the local vapor quality, mass flux, and saturation properties. This provides a smooth transition between predominantly convective and predominantly nucleate boiling regimes in the economizer.

5.7.3 Tube bank stages

For completeness, the water side model also includes correlations for cross flow over tube banks on the cold side (kind = "tube_bank"), although in the present thesis these stages are operated in pool boiling mode (so that only the Cooper correlation is used). When a tube bank description is required on the water side, the geometry is:

- tube outer diameter: D_o ,
- cold-side flow area: $A_{\text{cold,flow}}$,
- number of rows: N_{rows} ,
- transverse and longitudinal pitches: S_T, S_L ,
- bundle arrangement: inline or staggered.

The water velocity, Reynolds and Prandtl numbers are:

$$V_w = \frac{\dot{m}_w}{\rho_w A_{\text{cold,flow}}}, \quad (5.69)$$

$$\text{Re}_w = \frac{\rho_w V_w D_o}{\mu_w}, \quad \text{Pr}_w = \frac{c_{p,w} \mu_w}{k_w}. \quad (5.70)$$

A Zukauskas-type banded correlation is then applied:

$$\text{Nu}_w = C \text{Re}_w^m \text{Pr}_w^n, \quad (5.71)$$

[2] where:

- C, m are selected from standard Zukauskas bands based on Re_w and the arrangement (inline or staggered),
- the exponent n is

$$n = \begin{cases} 0.36, & \text{Pr}_w \leq 10 \\ 0.25, & \text{Pr}_w > 10 \end{cases} \quad (5.72)$$

The raw Nusselt number is further modified by:

- a row factor $f_{\text{row}}(N_{\text{rows}})$ that accounts for the finite number of tube rows, and
- a spacing factor $\phi(S_T, S_L, D_o)$ that accounts for maximum velocity effects in the tube bank (greater constriction \Rightarrow higher HTC).

If Re_w falls outside the Zukauskas validity range, the model falls back to the Churchill Bernstein correlation for cross flow over a single cylinder:

$$\text{Nu}_w = 0.3 + \frac{0.62 \text{Re}_w^{1/2} \text{Pr}_w^{1/3}}{\left[1 + (0.4/\text{Pr}_w)^{2/3}\right]^{1/4}} \left[1 + \left(\frac{\text{Re}_w}{282000}\right)^{5/8}\right]^{4/5}. \quad (5.73)$$

[2]

The corresponding water side HTC for a tube-bank configuration is:

$$h_{w,\text{conv}}^{(\text{bank})} = \frac{\text{Nu}_w k_w}{D_o}. \quad (5.74)$$

[2]

When such a tube bank model is used inside the Chen formulation, h_{lo} is taken from this $h_{w,\text{conv}}^{(\text{bank})}$.

5.7.4 Single tube and reversal chamber stages

Stages of kind `single_tube` and `reversal_chamber` correspond, on the water side, to external flow around one or more tubes within the drum/shell region. In the current thesis these are also operated in pool boiling mode (`pool_boiling = true`), so the Cooper pool boiling correlation described in the general formulation dominates their behavior. Nevertheless, the implementation includes external forced convection correlations for completeness.

For these stages the characteristic length for the water side is the tube outer diameter D_o , and the cold side flow area $A_{\text{cold,flow}}$ is defined by the drum cross section minus the tube area(s). When a cross flow description is used for single-phase or liquid only HTC:

- water velocity, Reynolds and Prandtl numbers:

$$V_w = \frac{\dot{m}_w}{\rho_w A_{\text{cold,flow}}}, \quad (5.75)$$

$$\text{Re}_w = \frac{\rho_w V_w D_o}{\mu_w}, \quad \text{Pr}_w = \frac{c_{p,w} \mu_w}{k_w}. \quad (5.76)$$

For a single tube in cross flow (or, by approximation, a relatively open bundle) a Churchill Bernstein style correlation is used:

$$\text{Nu}_w = 0.3 + \frac{0.62 \text{Re}_w^{1/2} \text{Pr}_w^{1/3}}{\left[1 + (0.4/\text{Pr}_w)^{2/3}\right]^{1/4}} \left[1 + \left(\frac{\text{Re}_w}{282000}\right)^{5/8}\right]^{4/5}, \quad (5.77)$$

[2] leading to

$$h_{w,\text{conv}}^{(\text{single})} = \frac{\text{Nu}_w k_w}{D_o}. \quad (5.78)$$

In reversal chamber segments, the tubes are bent, and the model applies the same base correlation multiplied by a curvature (bend) factor:

$$h_{w,\text{conv}}^{(\text{rev})} = \phi_{\text{bend}}(D_o, R_c) \frac{\text{Nu}_w k_w}{D_o}, \quad (5.79)$$

where R_c is the bend radius and $\phi_{\text{bend}} \geq 1$ is a modest enhancement (up to roughly 1.25) for tight bends, reflecting locally increased turbulence around the bend region.

In pool boiling operation these external convection correlations are only used implicitly inside the liquid only component h_{l_0} when the Chen type formulation is invoked. For the main boiling sections in this thesis, however, the water side is predominantly controlled by the Cooper pool boiling correlation with $T_w = T_{\text{sat}}(p)$.

Chapter 6

Hydraulic Model

Hydraulic behavior is extracted directly from the solver through the per step pressure drop decomposition implemented in `heat/solver.py` (`_gas_dp_components`, `pressure_drop_gas`) and accumulated at the stage level in `heat/solver.py::solve_stage`.

The model divides pressure losses into:

- Frictional losses
- Minor losses (inlet, outlet, bends, etc.)
- Total pressure drop (sum of the above)

6.1 Frictional losses

Gas and water sides

The per step frictional pressure drop follows a standard 1D Darcy formulation:

$$\Delta P_{\text{fric}} = -f \frac{\Delta x}{D_h} \left(\frac{\rho V^2}{2} \right) \quad (6.1)$$

[15]

Here:

- f is the Darcy friction factor,
- D_h is the relevant side hydraulic diameter ($D_h = \text{hot_Dh}$ for gas, $D_h = \text{cold_Dh}$ for water),
- ρ and V are local density and velocity on the relevant side,
- Δx is the current marching step length.

The friction factor is computed from Reynolds number and relative roughness via `_friction_factor`:

- Laminar ($\text{Re} < 2300$):

$$f = \frac{64}{\text{Re}} \quad (6.2)$$

[15]

- Transitional ($2300 \leq \text{Re} < 4000$): linear blend between laminar and turbulent values:

$$f = (1 - w)f_{\text{lam}} + wf_{\text{turb}}, \quad w = \frac{\text{Re} - 2300}{4000 - 2300} \quad (6.3)$$

[1]

- Turbulent ($\text{Re} \geq 4000$): Colebrook–White is solved iteratively, seeded by the Swamee–Jain explicit approximation.

Swamee–Jain seed (used as the initial guess):

$$f_{\text{SJ}} = \frac{0.25}{\left[\log_{10} \left(\frac{\varepsilon/D_h}{3.7} + \frac{5.74}{\text{Re}^{0.9}} \right) \right]^2} \quad (6.4)$$

[13]

Colebrook–White equation solved iteratively in the code:

$$\frac{1}{\sqrt{f}} = -2 \log_{10} \left(\frac{\varepsilon/D_h}{3.7} + \frac{2.51}{\text{Re}\sqrt{f}} \right) \quad (6.5)$$

[15]

The iteration is performed on $1/\sqrt{f}$ until convergence.

Local velocity and Reynolds number are evaluated using the side flow area A and properties:

$$V = \frac{\dot{m}}{\rho A}, \quad \text{Re} = \frac{\rho V D_h}{\mu} \quad (6.6)$$

Frictional losses are only applied for the economizer water side branch in `_water_dp_components`; for other stage kinds the current model sets $\Delta P_{\text{fric}} = 0$.

6.2 Gas side pressure drop in the economizer

The economizer gas side hydraulics differ fundamentally from all other modeled stages.

While other stages assume internal flow and apply a Darcy–Weisbach formulation, the economizer models external crossflow over a tube bank, and gas side pressure losses

are therefore computed using a bundle loss (drag-based) formulation rather than a wall-friction model.

Crossflow bundle formulation

The gas flows across a bank of tubes arranged either inline or staggered. A characteristic velocity is defined using a bulk velocity corrected by a geometry-dependent maximum-velocity factor:

$$V_{\text{bulk}} = \frac{\dot{m}}{\rho A_{\text{hot}}}, \quad V_{\text{char}} = u_{\max} V_{\text{bulk}} \quad (6.7)$$

where:

- A_{hot} = hot_flow_A is the free crossflow area,
- u_{\max} = umax_factor accounts for flow acceleration between tubes.

The Reynolds number is formed using the tube outer diameter:

$$\text{Re}_D = \frac{\rho V_{\text{char}} D_o}{\mu} \quad (6.8)$$

Bundle loss coefficient

The pressure loss per tube row is expressed via a dimensionless bundle loss coefficient:

$$\zeta_{\text{row}} = C_0 \text{Re}_D^m \Phi_{\text{geom}} \quad (6.9)$$

where:

- C_0 and m depend on tube arrangement (inline or staggered),
- Φ_{geom} accounts for pitch ratios:

$$\Phi_{\text{geom}} = \left(\frac{S_T/D_o}{1.5} \right)^{-0.2} \left(\frac{S_L/D_o}{1.5} \right)^{-0.2} \quad (6.10)$$

with transverse pitch S_T and longitudinal pitch S_L .

The total bundle loss coefficient is then:

$$\zeta_{\text{bundle}} = N_{\text{rows}} \zeta_{\text{row}} \quad (6.11)$$

where N_{rows} is the number of tube rows in the flow direction.

Distributed pressure loss

The dynamic pressure is evaluated using the characteristic velocity:

$$q = \frac{\rho V_{\text{char}}^2}{2} \quad (6.12)$$

The total bundle pressure drop is:

$$\Delta P_{\text{bundle}} = -\zeta_{\text{bundle}} q \quad (6.13)$$

This loss is distributed uniformly along the economizer length L across the marching steps:

$$\Delta P_{\text{fric,step}} = \Delta P_{\text{bundle}} \frac{\Delta x}{L} \quad (6.14)$$

where Δx is the local marching step length.

6.3 Minor losses

Minor losses are applied using per-stage catalogue K values and the standard dynamic-pressure formulation:

$$\Delta P_{\text{minor}} = -K_{\text{minor}} \left(\frac{\rho V^2}{2} \right) \quad (6.15)$$

[1]

The total minor-loss coefficient K_{minor} is assembled differently for gas and water sides, but applied through the same formulation.

Coefficient assembly

Gas side.

For each stage, the total loss coefficient is assembled from geometry and user inputs:

$$K_{\text{minor}} = K_{\text{contraction}} + K_{\text{expansion}} + K_{\text{bend}} \quad (6.16)$$

Where:

- $K_{\text{contraction}}$: accounts for sudden expansion of flow area (e.g. $\text{HX}_2 \rightarrow \text{HX}_3$), default = 0.5.
- $K_{\text{expansion}}$ (Borda–Carnot): losses caused by sudden expansion of flow area (e.g. $\text{HX}_1 \rightarrow \text{HX}_2$), default = 1.
- K_{bend} : losses due to gas flow rotation in reversal chambers, default = 0.

The bend loss is distributed uniformly across the n marching steps:

$$K_{\text{bend,per-step}} = \frac{K_{\text{cold,bend}}}{n} \quad (6.17)$$

The per-step assembled coefficient is:

$$K_{\text{minor}} = K_{\text{bend,per-step}} + \mathbb{1}_{i=0} K_{\text{cold,inlet}} + \mathbb{1}_{i=n-1} K_{\text{cold,outlet}} \quad (6.18)$$

Application

For both gas and water sides, the minor-loss pressure drop is computed using the local dynamic pressure:

$$V = \frac{\dot{m}}{\rho A}, \quad q = \frac{\rho V^2}{2}, \quad \Delta P_{\text{minor}} = -K_{\text{minor}} q \quad (6.19)$$

where A is the relevant side flow area ($A = \text{cold_flow_A}$ for water, gas side area otherwise).

6.4 Total pressure drop

For each step, the total side pressure change is the sum of frictional and minor components:

$$\Delta P_{\text{total}} = \Delta P_{\text{fric}} + \Delta P_{\text{minor}} \quad (6.20)$$

[15]

This is what `pressure_drop_gas/water` return and what is applied to the streams in `update_gas/water_after_step`.

6.5 Coupling of ΔP into the energy solver

Gas/water pressure is updated step-wise using the same ΔP model:

$$P_{i+1} = P_i + \Delta P_{\text{total}}(P_i, T_i, \dots) \quad (6.21)$$

After each step:

1. The local gas/water state (T_i, P_i , composition) is used to evaluate ρ, μ, k , and c_p .
2. The friction factor and dynamic pressure are computed from these properties.
3. ΔP_{fric} and ΔP_{minor} are formed.
4. The updated pressure P_{i+1} is used for the next step.

In this way, compressibility enters through the pressure dependence of $\rho(T, P)$ and $\mu(T, P)$ and their effect on V , Re , and f .

Chapter 7

Performance

This section summarizes the boiler level performance obtained from the coupled combustion heat transfer simulation. All numerical values are extracted from the stages summary and boiler summary data produced by the post-processing step `heat/postproc.py`.

7.1 Solution procedure

For any given operating conditions, the main solver `run_boiler_case()` performs an outer fixed point iteration, on boiler efficiency, and water mass flow:

1. The combustion sub-model called by `Combustor.run()`, returns:
 - the lower heating value based firing rate P_{LHV} ,
 - the total combustion heat release Q_{in} ,
 - the adiabatic flame temperature T_{ad} ,
 - the fully burnt flue-gas stream at burner exit.
2. Given a current efficiency guess $\eta^{(n)}$ and the combustion result, the corresponding feedwater/steam mass flow $\dot{m}_w^{(n)}$ is computed by `_water_mass_from_efficiency()` as

$$h_{\text{in}} = h_{\text{fw}}(P_{\text{fw}}), \quad h_{\text{steam}} = h_g(P_{\text{fw}}), \quad (7.1)$$

$$\Delta h = h_{\text{steam}} - h_{\text{in}}, \quad (7.2)$$

$$Q_{\text{target}}^{(n)} = \eta^{(n)} Q_{\text{in}}, \quad (7.3)$$

$$\dot{m}_w^{(n)} = \frac{Q_{\text{target}}^{(n)}}{\Delta h}. \quad (7.4)$$

3. A WaterStream with mass flow $\dot{m}_w^{(n)}$ is created and passed, together with the combustion flue gas GasStream and the drum/stage definitions, to the multi stage heat exchanger solver `run_hx()`.
4. `run_hx()` returns per stage and boiler level summary tables.
5. The new efficiency estimate is set to the indirect efficiency,

$$\eta^{(n+1)} := \eta_{\text{indirect}}^{(n)}, \quad (7.5)$$

And the procedure is repeated until the change in water mass flow between iterations is below the specified tolerance

$$|\dot{m}_w^{(n)} - \dot{m}_w^{(n-1)}| < 10^{-3} \text{ kg/s}, \quad (7.6)$$

or a maximum number of iterations is reached.

At convergence, returning:

- converged water/steam mass flow $\dot{m}_{w,\text{base}}$,
- converged indirect efficiency $\eta_{\text{indirect,base}}$,

together with the corresponding boiler summary quantities (stack temperature, total pressure drop, etc.). These and more are exported to CSV as `boiler_summary.csv` and `stages_summary.csv`.

7.2 Energy balance

The total useful heat transferred from the flue gas to the water/steam side is obtained by integrating the local line heat flux $q'(x)$ over all stages:

$$Q_{\text{useful}} = \sum_{k=1}^6 Q_{\text{stage},k} = \sum_{k=1}^6 \int_q' (x) dx \quad (7.7)$$

The total input heat from combustion Q_{in} is taken from the combustion module as the rate of heat release from complete fuel burnout:

7.3 Efficiency

Two boiler efficiencies are reported:

- Direct efficiency (LHV):

$$\eta_{\text{direct}} = \frac{Q_{\text{useful}}}{P_{\text{LHV}}} \quad (7.8)$$

- Indirect efficiency:

$$\eta_{\text{indirect}} = 1 - \frac{Q_{\text{losses}}}{Q_{\text{in}}} \quad (7.9)$$

7.4 Water/Steam flow rate convergence

The water/steam mass flow rate is obtained iteratively from an assumed overall boiler efficiency and the combustion heat input. At each iteration n the code:

1. Assumes an efficiency $\eta^{(n)}$.
2. Computes the target useful duty:

$$Q_{\text{target}}^{(n)} = \eta^{(n)} Q_{\text{in}} \quad (7.10)$$

3. Determines the required water mass flow $\dot{m}_w^{(n)}$ from the enthalpy rise between feedwater and saturated steam at drum pressure:

$$\dot{m}_w^{(n)} = \frac{Q_{\text{target}}^{(n)}}{h_{\text{steam}}(P_{\text{drum}}) - h_{\text{fw}}} \quad (7.11)$$

4. Runs the full multi-stage heat-exchanger model with $\dot{m}_w^{(n)}$ and reads back the resulting indirect efficiency $\eta_{\text{indirect}}^{(n)}$.
5. Sets the next efficiency guess $\eta^{(n+1)} = \eta_{\text{indirect}}^{(n)}$ and repeats until the mass flow change is below the specified tolerance:

$$|\dot{m}_w^{(n)} - \dot{m}_w^{(n-1)}| < 10^{-3} \text{ kg/s} \quad (7.12)$$

Chapter 8

Performance Analysis

The purpose of this chapter is to evaluate the thermal and hydraulic performance of the developed fire tube shell boiler model under representative operating conditions and systematic parameter variations. The analysis aims to quantify how key controllable and design relevant parameters influence boiler efficiency, steam production, heat transfer distribution, and pressure losses.

8.1 Control case

The control case defines the nominal operating condition of the boiler and serves as the reference point for all subsequent parametric studies. It represents typical industrial operation, enabling direct comparison with published industrial boiler performance data. Defined by:

- Fuel mass flow: $\dot{m}_{\text{fuel}} = 0.1 \text{ kg s}^{-1}$
- Excess air ratio: $\lambda = 1.1$
- Drum pressure: $P_{\text{drum}} = 10 \text{ bar}$
- Fouling factor : $f = 1 \text{ [-]}$

All parameters not under investigation are held fixed at their control values during each parametric sweep.

Table 8.1: Control case performance.

control	control
Fuel Mass Flow[Kg/S]	0.1
Air Flow[Kg/S]	1.69
Excess Air Ratio[-]	1.05
Feedwater Flow[Kg/S]	1.89
Steam Capacity[T/H]	6.81
η_{direct} [-]	0.95
η_{indirect} [-]	0.95
Stack Loss Fraction[-]	0.05
Q_Flue_Out[Mw]	0.25
conductance [MW/K]	0.01

control	control
input heat [MW]	4.68
useful heat [MW]	4.42
Q_Balance_Error[Mw]	-0
Pressure Drop Fric Total[Kpa]	-8.35
Pressure Drop Minor Total[Kpa]	-4.09
Pressure Drop Total[Kpa]	-12.45
Water Pressure Drop Fric Total[Kpa]	-0.06
Water Pressure Drop Minor Total[Kpa]	-0
Water Pressure Drop Total[Kpa]	-0.06
Lhv [Mj/Kg]	46.73
firing rate [MW]	4.67
adiabatic temperature [°C]	1981.5
Stack Temperature[°C]	152.38
Feedwater Pressure[Kpa]	1000.06
Drum Pressure[Kpa]	1000

The performance (notably $\eta_{\text{direct}} = 0.95$ on an LHV basis and $T_{\text{stack}} = 152.4^{\circ}\text{C}$) was compared against published reference values for gas-fired fire tube boilers with economizer [], and found to be within expected tolerance ranges.

8.1.1 Stage-wise heat transfer and hydraulics

Stage-wise analysis is used to understand how heat transfer mechanisms and hydraulic behavior evolve along the gas path, and to verify whether parameter variations (excess air, fuel flow, drum pressure) introduce any regime changes between stages.

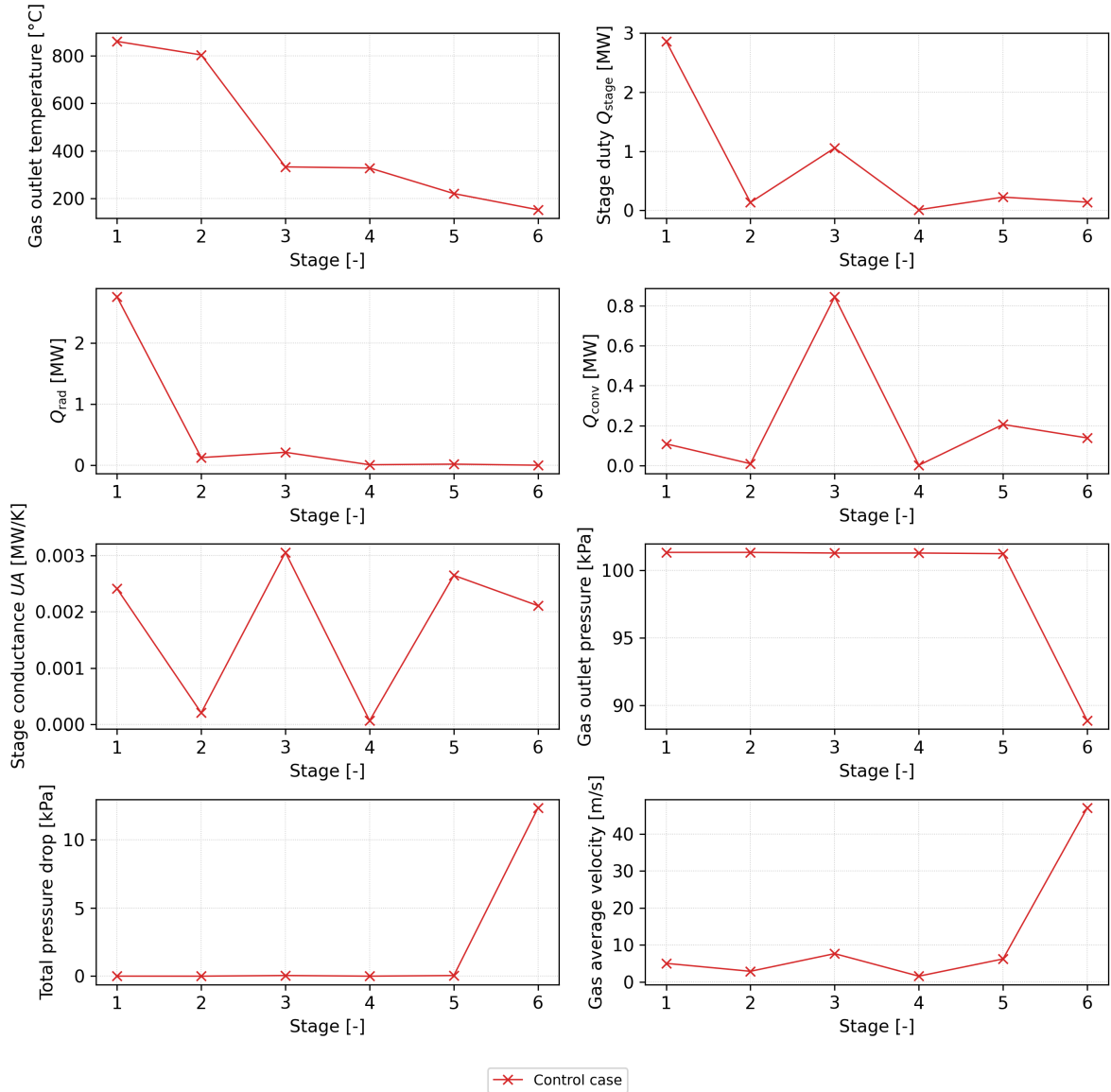


Figure 8.1: Stage wise heat transfer and hydraulic profiles

Across all runs the stage pattern stays the same: gas temperature drops from HX 1 to HX 6, stage heat duty is highest in the first stages and decreases downstream, and early stages are driven mainly by radiative transfer while later stages are relatively more convective.

Excess air primarily weakens and redistributes heat transfer by lowering upstream gas temperatures, reducing early-stage duties, shifting recovery downstream, and increasing gas velocity and total pressure drop. Fuel flow scales the entire system: higher fuel rates raise gas temperatures, stage duties, and both radiative and convective contributions, with the largest absolute impact in the furnace and first tube bank, while also increasing pressure losses. Drum pressure has a comparatively minor effect on gas-side behavior, mainly influencing downstream heat recovery through water-side conditions. Table: Control case stages summary.

stage KPI	HX_1	HX_2	HX_3	HX_4	HX_5	HX_6
Kind	Furnace	reversal	tube_bank	reversal	tube_bank	economizer
Gas In Pressure[Kpa]	101.33	101.32	101.32	101.27	101.27	101.23
Gas In Temp[°C]	1981.25	860.87	804.14	332.78	328.16	220.51
Gas In Enthalpy[Kj/Kg]	2612.29	1014.02	938.90	349.39	343.96	219.06
Gas Out Pressure[Kpa]	101.32	101.32	101.27	101.27	101.23	88.88
Gas Out Temp[°C]	860.87	804.14	332.78	328.16	220.51	152.38
Gas Out Enthalpy[Kj/Kg]	1014.02	938.90	349.39	343.96	219.06	141.69
Water In Temp[°C]	179.89	179.89	179.89	179.89	179.89	104.80
Water In Enthalpy[Kj/Kg]	762.68	762.68	762.68	762.68	762.68	440.00
Water In Pressure[Kpa]	1000.00	1000.00	1000.00	1000.00	1000.00	1000.06
Water Out Temp[°C]	179.89	179.89	179.89	179.89	179.89	122.09
Water Out Enthalpy[Kj/Kg]	762.68	762.68	762.68	762.68	762.68	513.21
Water Out Pressure[Kpa]	1000.00	1000.00	1000.00	1000.00	1000.00	1000.00
Gas Avg Velocity[M/S]	5.04	2.90	7.67	1.58	6.24	47.04
Water Avg Velocity[M/S]						0.03
Pressure Drop Fric[Kpa]	-0.00	-0.00	-0.03	-0.00	-0.03	-8.30
Pressure Drop Minor[Kpa]	-0.00	-0.00	-0.02	-0.00	-0.02	-4.05
Pressure Drop Total[Kpa]	-0.00	-0.00	-0.05	-0.00	-0.05	-12.35
Water Pressure Drop Fric[Kpa]						-0.06
Water Pressure Drop Minor[Kpa]						-0.00
Water Pressure Drop Total[Kpa]						-0.06
Q Conv[Mw]	0.11	0.01	0.84	0.00	0.21	0.14
Q Rad[Mw]	2.75	0.13	0.21	0.01	0.02	0.00
Q Total[Mw]	2.86	0.13	1.06	0.01	0.22	0.14
conductance [MW/K]	0.00	0.00	0.00	0.00	0.00	0.00
Steam Capacity[T/H]	4.55	0.21	1.68	0.02	0.36	

8.2 Results and parametric analysis

8.2.1 Influence of excess air factor

The excess air factor λ quantifies the ratio of supplied combustion air to the theoretical stoichiometric requirement. It directly affects combustion completeness, flue gas mass flow rate, adiabatic flame temperature, and stack losses, making it a key operational control parameter in industrial boilers. This parameter is investigated to assess the trade-off between combustion stability and thermal efficiency. The excess air ratio is varied over the range

$$\lambda = [1.00, 1.05, 1.10, 1.15, 1.20, 1.30] [-], \quad (8.1)$$

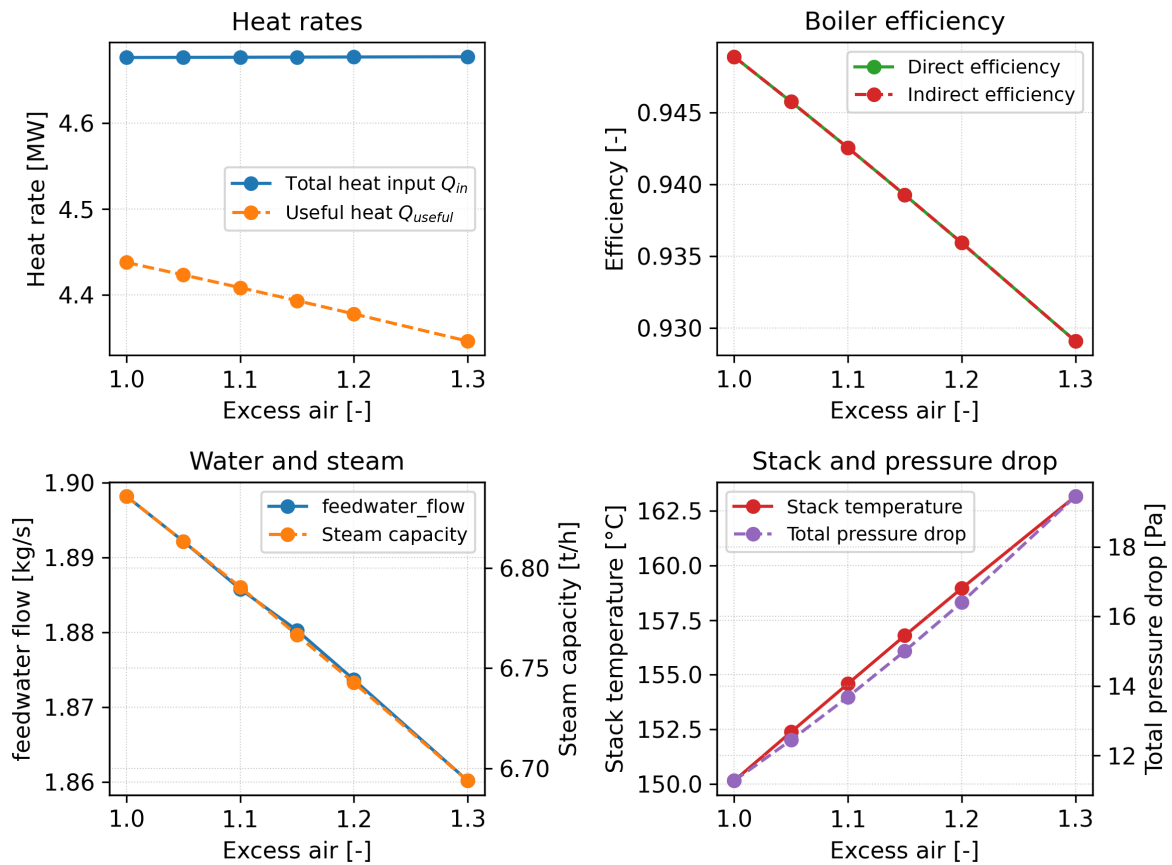


Figure 8.2: Boiler performance as a function of excess air factor

Increasing the excess air ratio increases flue-gas mass flow and sensible stack losses. As a result, boiler efficiency exhibits a maximum near the control value $\lambda = 1.05$, beyond which additional air primarily raises stack temperature and pressure losses without improving useful heat transfer.

Table 8.2: Excess air performance analysis.

excess air [-]	1.00	1.05	1.10	1.15	1.20	1.30
Fuel Mass Flow[Kg/S]	0.1	0.1	0.1	0.1	0.1	0.1
Air Flow[Kg/S]	1.61	1.69	1.77	1.85	1.93	2.09
Excess Air Ratio[-]	1	1.05	1.1	1.15	1.2	1.3
Feedwater Flow[Kg/S]	1.9	1.89	1.89	1.88	1.87	1.86
Steam Capacity[T/H]	6.84	6.81	6.79	6.77	6.74	6.69
η_{direct} [-]	0.95	0.95	0.94	0.94	0.94	0.93
$\eta_{indirect}$ [-]	0.95	0.95	0.94	0.94	0.94	0.93
Stack Loss Fraction[-]	0.05	0.05	0.06	0.06	0.06	0.07
Q_{Flue_Out} [Mw]	0.24	0.25	0.27	0.28	0.3	0.33
conductance [MW/K]	0.01	0.01	0.01	0.01	0.01	0.01
input heat [MW]	4.68	4.68	4.68	4.68	4.68	4.68
useful heat [MW]	4.44	4.42	4.41	4.39	4.38	4.35
$Q_{Balance_Error}$ [Mw]	-0	-0	-0	-0	-0	-0

excess air [-]	1.00	1.05	1.10	1.15	1.20	1.30
Pressure Drop Fric Total[Kpa]	-7.58	-8.35	-9.17	-10.05	-10.97	-12.97
Pressure Drop Minor Total[Kpa]	-3.7	-4.09	-4.51	-4.96	-5.44	-6.48
Pressure Drop Total[Kpa]	-11.28	-12.45	-13.69	-15.01	-16.4	-19.46
Water Pressure Drop Fric	-0.06	-0.06	-0.06	-0.06	-0.06	-0.05
Total[Kpa]						
Water Pressure Drop Minor	-0	-0	-0	-0	-0	-0
Total[Kpa]						
Water Pressure Drop Total[Kpa]	-0.06	-0.06	-0.06	-0.06	-0.06	-0.06
Lhv [Mj/Kg]	46.73	46.73	46.73	46.73	46.73	46.73
firing rate [MW]	4.67	4.67	4.67	4.67	4.67	4.67
adiabatic temperature [°C]	2052.36	1981.5	1915.54	1854.03	1796.53	1692.05
Stack Temperature[°C]	150.16	152.38	154.59	156.79	158.95	163.16
Feedwater Pressure[Kpa]	1000.06	1000.06	1000.06	1000.06	1000.06	1000.06
Drum Pressure[Kpa]	1000	1000	1000	1000	1000	1000

8.2.2 Influence of fuel mass flow

The fuel mass flow rate \dot{m}_{fuel} determines the firing rate of the boiler and therefore governs the total thermal input, flue gas temperature level, and achievable steam production capacity. It is a primary load-setting parameter in boiler operation and is investigated to evaluate how the system scales with increasing and decreasing demand. The fuel mass flow is varied according to

$$\dot{m}_{\text{fuel}} = [0.025, 0.050, 0.075, 0.10, 0.125] \frac{\text{kg}}{\text{s}}, = [25, 50, 75, 100, 125] \% \quad (8.2)$$

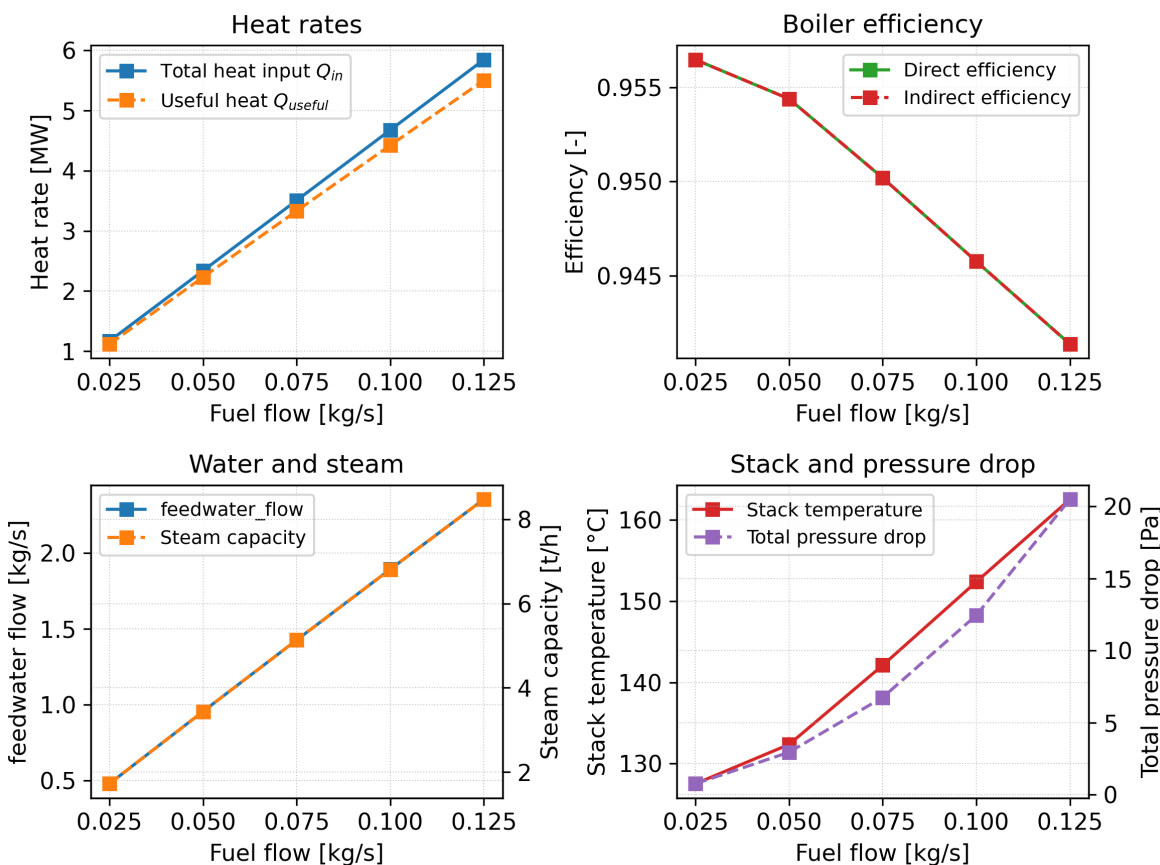


Figure 8.3: Boiler performance as a function of fuel mass flow

Steam capacity increases approximately linearly with fuel input, indicating that the available heat transfer surface is sufficient to absorb the additional duty. As the firing rate approaches the nominal design value, deviations from linearity become apparent, reflecting increasing limitations in heat transfer effectiveness rather than fuel input.

Table 8.3: Fuel flow performance analysis.

fuel flow [kg/s]	0.02	0.05	0.08	0.10	0.12
Fuel Mass Flow[Kg/S]	0.02	0.05	0.08	0.1	0.12
Air Flow[Kg/S]	0.42	0.85	1.27	1.69	2.11
Excess Air Ratio[-]	1.05	1.05	1.05	1.05	1.05
Feedwater Flow[Kg/S]	0.48	0.95	1.43	1.89	2.35
Steam Capacity[T/H]	1.72	3.44	5.13	6.81	8.48
η_{direct} [-]	0.96	0.95	0.95	0.95	0.94
η_{indirect} [-]	0.96	0.95	0.95	0.95	0.94
Stack Loss Fraction[-]	0.04	0.05	0.05	0.05	0.06
Q_Flue_Out[Mw]	0.05	0.11	0.17	0.25	0.34
conductance [MW/K]	0	0.01	0.01	0.01	0.01
input heat [MW]	1.17	2.34	3.51	4.68	5.85
useful heat [MW]	1.12	2.23	3.33	4.42	5.5
Q_Balance_Error[Mw]	-0	-0	-0	-0	-0
Pressure Drop Fric Total[Kpa]	-0.54	-2.02	-4.57	-8.35	-13.65
Pressure Drop Minor Total[Kpa]	-0.23	-0.93	-2.18	-4.09	-6.84
Pressure Drop Total[Kpa]	-0.77	-2.95	-6.75	-12.45	-20.49
Water Pressure Drop Fric Total[Kpa]	-0.01	-0.02	-0.03	-0.06	-0.11
Water Pressure Drop Minor	-0	-0	-0	-0	-0
Total[Kpa]					
Water Pressure Drop Total[Kpa]	-0.01	-0.02	-0.03	-0.06	-0.11
Lhv [Mj/Kg]	46.73	46.73	46.73	46.73	46.73
firing rate [MW]	1.17	2.34	3.5	4.67	5.84
adiabatic temperature [°C]	1981.5	1981.5	1981.5	1981.5	1981.5
Stack Temperature[°C]	127.53	132.36	142.11	152.38	162.54
Feedwater Pressure[Kpa]	1000.01	1000.02	1000.03	1000.06	1000.11
Drum Pressure[Kpa]	1000	1000	1000	1000	1000

8.2.3 Influence of drum pressure

The drum pressure P_{drum} determines the saturation temperature and latent heat of vaporization of water, thereby influencing steam generation characteristics and the available temperature driving force for heat transfer. This parameter is investigated to quantify how changes in operating pressure affect boiler efficiency, steam capacity, and stack temperature. The drum pressure is varied over the range

$$P_{\text{drum}} = [4.0, 10.0, 16.0] \text{ bar}, \quad (8.3)$$

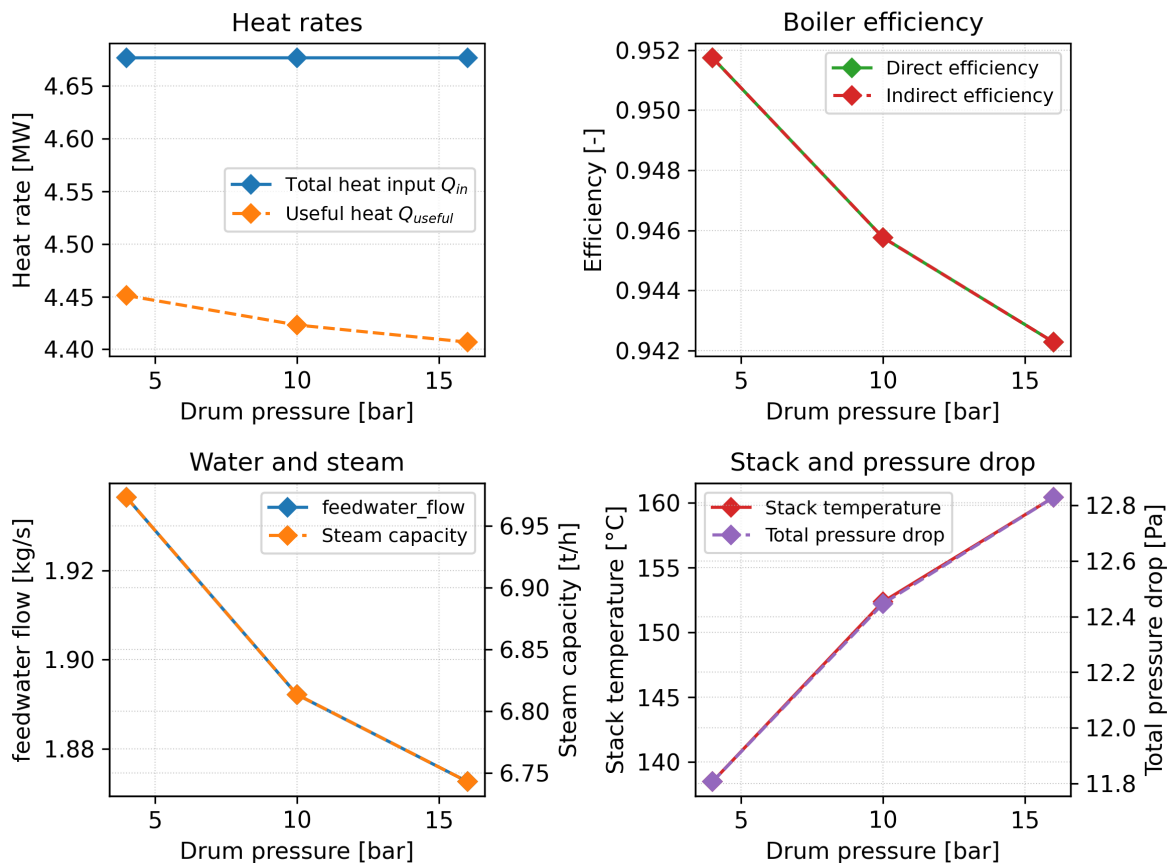


Figure 8.4: Boiler performance as a function of drum pressure

Increasing the drum pressure, allows a larger steam mass flow to be generated for the same absorbed thermal duty. The direct efficiency decreases, since higher water and steam temperatures reduce the available driving temperature difference on the gas side. Consistent with this, the stack temperature increases, indicating a diminished potential for further heat recovery.

Table 8.4: Drum pressure performance analysis.

drum pressure [bar]	4.00	10.00	16.00
Fuel Mass Flow[Kg/S]	0.1	0.1	0.1

drum pressure [bar]	4.00	10.00	16.00
Air Flow[Kg/S]	1.69	1.69	1.69
Excess Air Ratio[-]	1.05	1.05	1.05
Feedwater Flow[Kg/S]	1.94	1.89	1.87
Steam Capacity[T/H]	6.97	6.81	6.74
η_{direct} [-]	0.95	0.95	0.94
η_{indirect} [-]	0.95	0.95	0.94
Stack Loss Fraction[-]	0.05	0.05	0.06
Q_Flue_Out[Mw]	0.23	0.25	0.27
conductance [MW/K]	0.01	0.01	0.01
input heat [MW]	4.68	4.68	4.68
useful heat [MW]	4.45	4.42	4.41
Q_Balance_Error[Mw]	-0	-0	-0
Pressure Drop Fric Total[Kpa]	-7.91	-8.35	-8.62
Pressure Drop Minor Total[Kpa]	-3.9	-4.09	-4.21
Pressure Drop Total[Kpa]	-11.81	-12.45	-12.83
Water Pressure Drop Fric Total[Kpa]	-0.06	-0.06	-0.06
Water Pressure Drop Minor Total[Kpa]	-0	-0	-0
Water Pressure Drop Total[Kpa]	-0.06	-0.06	-0.06
Lhv [Mj/Kg]	46.73	46.73	46.73
firing rate [MW]	4.67	4.67	4.67
adiabatic temperature [°C]	1981.5	1981.5	1981.5
Stack Temperature[°C]	138.49	152.38	160.44
Feedwater Pressure[Kpa]	400.06	1000.06	1600.06
Drum Pressure[Kpa]	400	1000	1600

8.2.4 Influence of fouling

The fouling factor f represents the degradation of effective heat transfer performance caused by deposits on gas-side and water-side heat exchange surfaces during operation, as dimensionless fouling thickness multiplier. Fouling increases thermal resistance, reduces overall heat transfer coefficients, and can significantly impact efficiency and stack losses over time. This parameter is investigated to assess the sensitivity of boiler performance to surface degradation. The fouling factor is varied as

$$f = [0.5\times, 1\times, 2\times, 5\times, 10\times]. \quad (8.4)$$

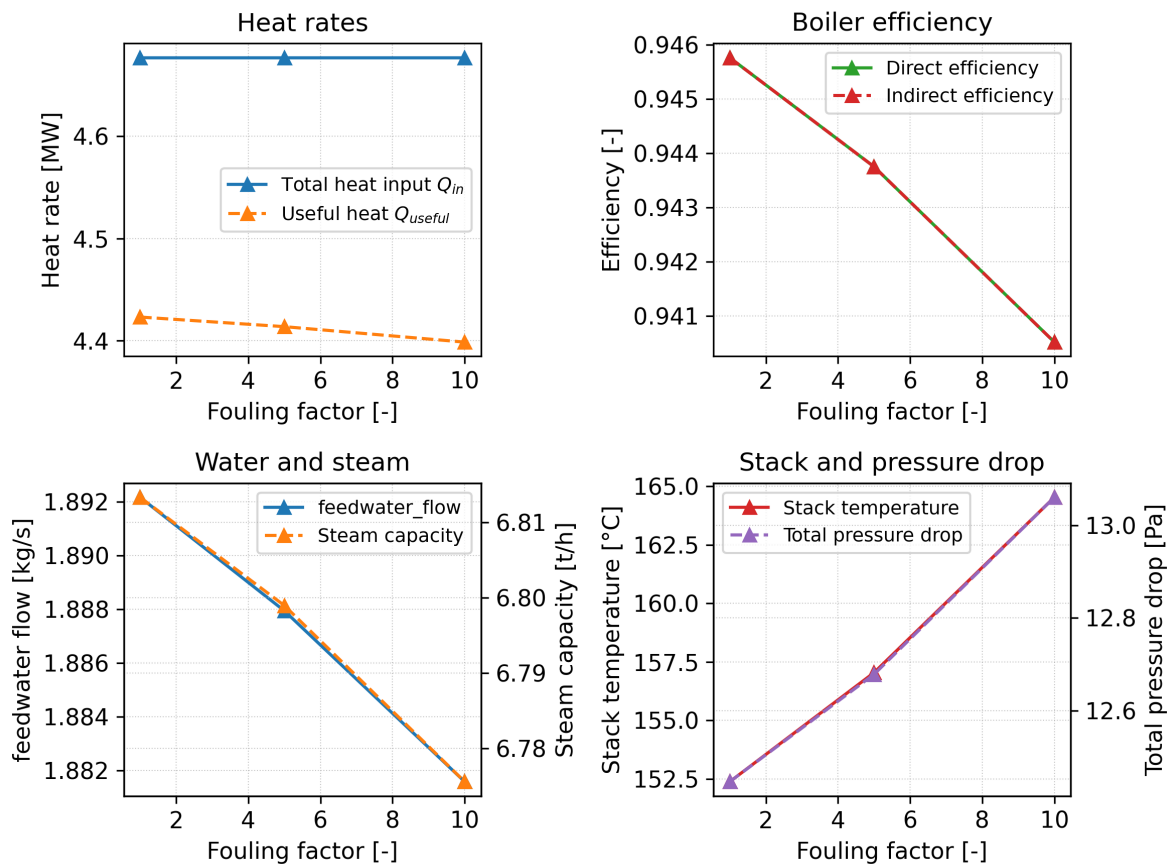


Figure 8.5: Boiler performance as a function of fouling factor

The effect of fouling is distributed across all stages, but its impact is most pronounced in the downstream convective sections where heat transfer is already limited by smaller temperature differences. As fouling increases, these sections lose effectiveness first.

While the boiler can continue to operate under fouled conditions, the results highlight the importance of maintaining clean heat transfer surfaces to ensure higher efficiency.

Table 8.5: Fouling performance analysis.

fouling [-]	1.00	5.00	10.00
Fuel Mass Flow[Kg/S]	0.1	0.1	0.1
Air Flow[Kg/S]	1.69	1.69	1.69
Excess Air Ratio[-]	1.05	1.05	1.05
Feedwater Flow[Kg/S]	1.89	1.89	1.88
Steam Capacity[T/H]	6.81	6.8	6.78
η_{direct} [-]	0.95	0.94	0.94
η_{indirect} [-]	0.95	0.94	0.94
Stack Loss Fraction[-]	0.05	0.06	0.06
Q_Flue_Out[Mw]	0.25	0.26	0.28
conductance [MW/K]	0.01	0.01	0.01
input heat [MW]	4.68	4.68	4.68
useful heat [MW]	4.42	4.41	4.4
Q_Balance_Error[Mw]	-0	-0	-0
Pressure Drop Fric Total[Kpa]	-8.35	-8.51	-8.77
Pressure Drop Minor Total[Kpa]	-4.09	-4.17	-4.29
Pressure Drop Total[Kpa]	-12.45	-12.68	-13.06
Water Pressure Drop Fric Total[Kpa]	-0.06	-0.06	-0.06
Water Pressure Drop Minor Total[Kpa]	-0	-0	-0
Water Pressure Drop Total[Kpa]	-0.06	-0.06	-0.06
Lhv [Mj/Kg]	46.73	46.73	46.73
firing rate [MW]	4.67	4.67	4.67
adiabatic temperature [°C]	1981.5	1981.5	1981.5
Stack Temperature[°C]	152.38	157.04	164.53
Feedwater Pressure[Kpa]	1000.06	1000.06	1000.06
Drum Pressure[Kpa]	1000	1000	1000

8.3 Conclusions from performance analysis

This section summarizes the main findings of the parametric performance analysis and highlights the relative influence of key operating parameters on boiler behavior and efficiency.

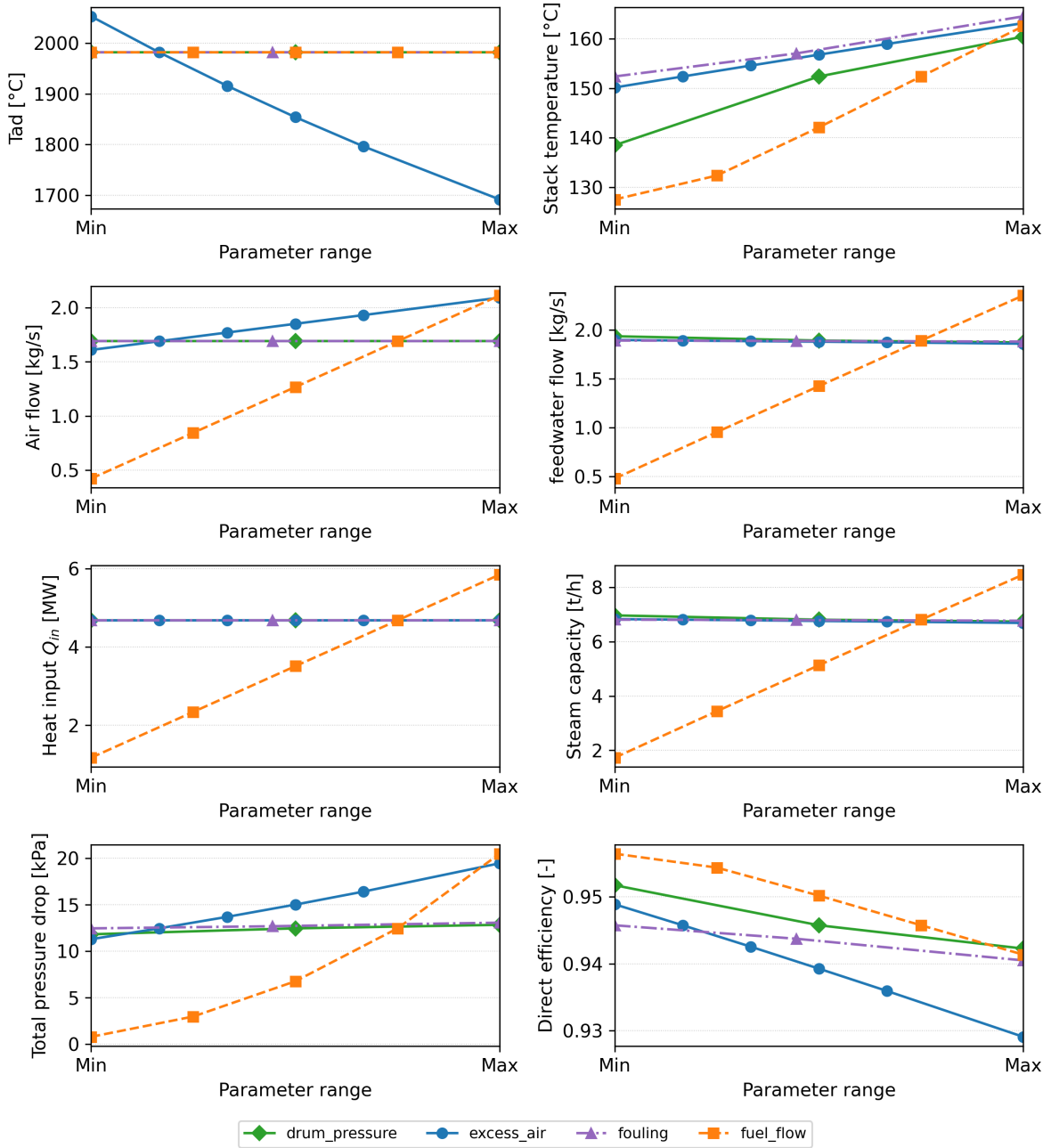


Figure 8.6: Overview of key boiler performance indicators for all parameter groups

Overall, the results show that fuel flow is the dominant factor affecting boiler performance. Increasing fuel flow strongly increases heat input, steam production, stack temperature, pressure drop, and leads to a noticeable reduction in direct efficiency at higher values. In contrast, changes in excess air, drum pressure, and fouling mainly cause smaller, secondary shifts, primarily influencing stack temperature and efficiency, but leave most other boiler variables relatively unchanged.

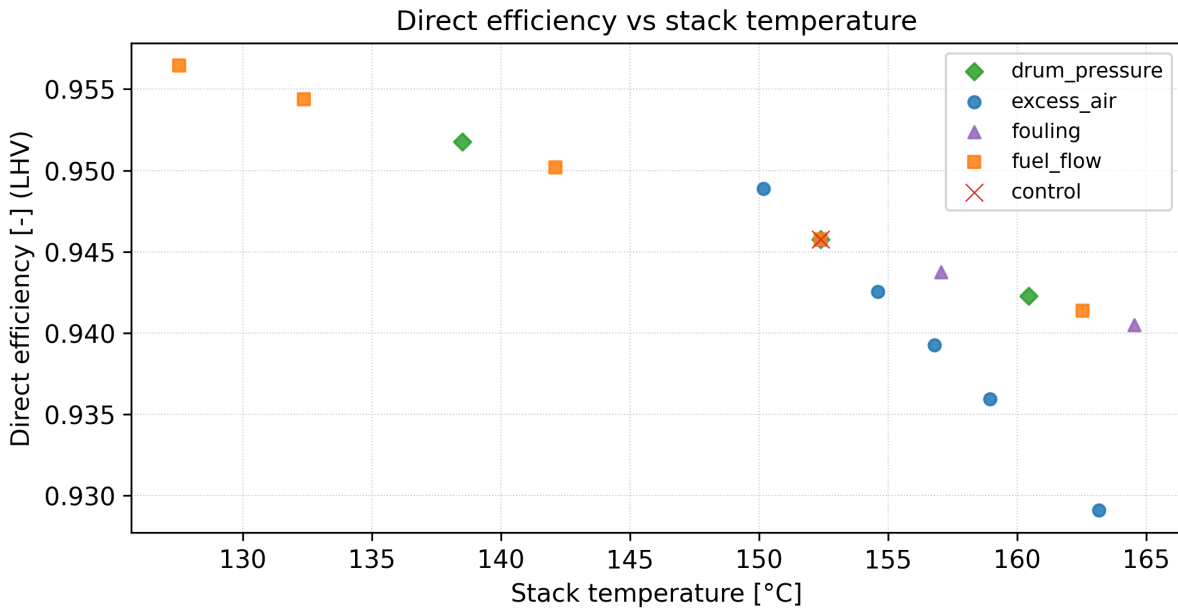


Figure 8.7: Scatter diagram showing stack temperature and direct efficiency

The parametric analysis demonstrates that the developed boiler model captures physically consistent trends across a wide range of operating conditions.

The excess air ratio is identified as the most influential parameter affecting boiler efficiency, primarily through its control of flue-gas mass flow, adiabatic flame temperature, and stack losses. An efficiency optimum is observed near the nominal excess air setting, consistent with industrial practice.

Fuel mass flow primarily scales the thermal duty and steam production rate, with efficiency remaining nearly constant over the investigated range. This indicates that, within practical limits, the available heat transfer surface is sufficient to accommodate load variations without significant degradation in performance.

Drum pressure mainly influences steam generation through changes in latent heat and saturation temperature, while its effect on overall efficiency is secondary. Higher pressures reduce the temperature driving force for heat transfer, resulting in elevated stack temperatures.

Fouling degrades heat transfer effectiveness across all stages, with the strongest impact observed in downstream convective sections. The results highlight the importance of maintaining clean heat transfer surfaces to preserve efficiency and minimize stack losses.

Overall, the analysis confirms that the coupled combustion–heat transfer–hydraulic framework provides a robust tool for evaluating operational trade-offs and identifying efficiency-critical parameters in industrial fire tube shell boilers.

Chapter 9

Summary

This thesis presented a physics based modelling framework for a three pass fire tube industrial shell boiler, integrating combustion, heat transfer, and hydraulic behavior within a single tool. The model was implemented in Python and structured around a one dimensional marching solver that resolves gas side and water/steam side processes consistently along the boiler flow path.

The developed framework couples three main sub models:

- A detailed fuel air combustion model.
- Heat transfer is resolved across six sequential gas side stages.
- Gas side pressure losses are computed concurrently with heat transfer, Water side pressure losses are evaluated for the economizer circuit.

The performance analysis demonstrates that boiler efficiency is most sensitive to the excess air ratio, which directly controls flue gas mass flow, adiabatic flame temperature, and stack losses. The firing rate primarily governs the absolute thermal duty and steam production. Drum pressure mainly influences steam quantity through its effect on latent heat and saturation temperature, while having only a secondary impact on overall thermal efficiency; higher pressures reduce the available temperature driving force, elevating stack temperatures.

Across all cases, the coupled model captures the interplay between combustion conditions, heat transfer effectiveness, and hydraulic constraints, providing a physically consistent basis for assessing operational trade offs and identifying efficiency critical control parameters in industrial fire tube boilers.

Appendix A

config and input

Air Properties (*config/air.yaml*)

Table A.1: Air parameters.

Quantity / Species	Symbol	Value	Units
Temperature	T	300.0	K
Pressure	P	101325	Pa
Oxygen (molar fraction)	x_{O_2}	0.23067	(–)
Nitrogen (molar fraction)	x_{N_2}	0.755866	(–)
Argon (molar fraction)	x_{Ar}	0.01287	(–)
Carbon dioxide (molar fraction)	x_{CO_2}	0.000594	(–)
Water vapour (molar fraction)	x_{H_2O}	0.0	(–)

Drum Geometry and Wall Properties (*config/drum.yaml*)

Table A.2: Drum parameters.

Quantity	Symbol	Value	Units
Inner diameter	D_{drum}	4.5	m
Length	L_{drum}	5.0	m
Wall thickness	δ_{wall}	0.05	m
Wall thermal conductivity	k_{wall}	40	$W m^{-1} K^{-1}$
Inner surface roughness	ε	5	μm
Inner surface emissivity	ε_r	0.80	(–)
Fouling thickness	δ_f	1.0×10^{-4}	m
Fouling conductivity	k_f	0.2	$W m^{-1} K^{-1}$

Fuel Properties (*config/fuel.yaml*)

Table A.3: Fuel parameters.

Quantity / Species	Symbol	Value	Units
Temperature	T	300.0	K
Pressure	P	101325	Pa
Mass flow rate	\dot{m}_{fuel}	0.1	kg s^{-1}
Methane (molar fraction)	CH_4	0.849546	(—)
Ethane (molar fraction)	C_2H_6	0.061889	(—)
Propane (molar fraction)	C_3H_8	0.020597	(—)
Butane (molar fraction)	C_4H_{10}	0.005154	(—)
Hydrogen sulfide (molar fraction)	H_2S	0.000103	(—)
Nitrogen (molar fraction)	N_2	0.041293	(—)
Carbon dioxide (molar fraction)	CO_2	0.016418	(—)
Water (molar fraction)	H_2O	0.005	(—)
Argon (molar fraction)	Ar	0.0	(—)

Operating Conditions (*config/operation.yaml*)

Table A.4: Operation parameters.

Quantity	Symbol	Value	Units
Excess air ratio	λ	1.1	(—)
Drum pressure	P_{drum}	10	bar

Heat Exchange Stages (*config/stages.yaml*)

Table A.5: Stages parameters.

Quantity	Symbol	HX-1	HX-2	HX-3	HX-4	HX-5	HX-6	Units
Inner diameter	D_i	1.4	1.6	0.076	1.6	0.076	0.0337	m
Inner / tube length	L_i, L	5.276	0.8	4.975	0.8	5.620	80	m
Wall thickness	δ	0.02	—	—	—	—	—	m
Thermal conductivity	k	50	—	—	—	—	—	$\text{W m}^{-1} \text{K}^{-1}$

Quantity	Symbol	HX- 1	HX- 2	HX- 3	HX- 4	HX- 5	HX- 6	Units
Curvature radius	R	—	0.8	—	0.8	—	—	m
Number of tubes	N	—	—	118	—	100	60	(—)
Number of rows	N_{rows}	—	—	6	—	6	20	(—)
Number of circuits	n_c	—	—	—	—	—	4	(—)
Transverse pitch	S_T	—	—	0.11	—	0.11	0.09	m
Longitudinal pitch	S_L	—	—	0.11	—	0.11	0.10	m
Baffle spacing	B	—	—	0.45	—	0.45	0.25	m
Baffle cut	c	—	—	0.25	—	0.25	0.25	(—)
Bundle clearance	—	—	—	0.010	—	0.010	0.010	m
Shell inner diameter	D_{shell}	—	—	—	—	—	0.95	m
Hot inlet loss	$K_{\text{hot,in}}$	0.5	—	0.5	—	0.5	0.5	(—)
Hot outlet loss	$K_{\text{hot,out}}$	0.0	—	1.0	—	1.0	1.0	(—)
Hot bend loss	$K_{\text{hot,bend}}$	0.0	0.3	—	0.3	—	—	(—)
Cold inlet loss	$K_{\text{cold,in}}$	0.0	—	—	—	—	0.5	(—)
Cold outlet loss	$K_{\text{cold,out}}$	0.0	—	—	—	—	1.0	(—)
Cold bend loss	$K_{\text{cold,bend}}$	0.0	—	—	—	—	0.3	(—)

Water Properties (*config/water.yaml*)

Table A.6: Water parameters.

Quantity	Symbol	Value	Units
Specific enthalpy	h	4.40×10^5	J kg^{-1}
Composition	$x_{\text{H}_2\text{O}}$	1.0	(—)

Appendix B

Results summary

Appendix C

Codebase

References

- [1] Crane Co. *Flow of Fluids Through Valves, Fittings, and Pipe (Technical Paper No. 410)*. 25th ed. Crane Company, 2018.
- [2] Frank P. Incropera et al. *Fundamentals of Heat and Mass Transfer*. 7th ed. Wiley, 2011.
- [3] International Organization for Standardization. *ISO 6976: Natural Gas – Calculation of Calorific Values, Density, Relative Density and Wobbe Index*. Tech. rep. Geneva, Switzerland: ISO, 2016.
- [4] Ferenc Lezovits. *Lecture 7: Heat Boilers*. Lecture slides, BMEEENBGHG: Heat Engines, Budapest University of Technology and Economics. 2022.
- [5] Make Boiler. *Industrial Boiler Cross-Section Diagram*. Cross-sectional schematic of an industrial shell boiler. Make Boiler. 2025. URL: <https://www.makeboiler.com/wp-content/uploads/2025/08/1-1024x563.jpg> (visited on 01/09/2026).
- [6] Make Piping Easy. *Economizer Tube Bundle Cross-Section*. Image used as reference for economizer cross-section. Make Piping Easy. 2024. URL: <https://makepipingeasy.com/wp-content/uploads/2024/11/1000047648-1024x506.jpg> (visited on 01/09/2026).
- [7] Bonnie J. McBride, Sanford Gordon, and Marc A. Reno. *Coefficients for Calculating Thermodynamic and Transport Properties of Individual Species*. Tech. rep. NASA/TP–2002-211556. Includes standard dry air composition used in combustion and thermodynamic calculations. Cleveland, Ohio: NASA Glenn Research Center, 2002.
- [8] Bonnie J. McBride, Sanford Gordon, and Michael A. Reno. *Coefficients for Calculating Thermodynamic and Transport Properties of Individual Species*. NASA Reference Publication 1311. NASA Glenn Research Center, 1993.
- [9] Michael F. Modest. *Radiative Heat Transfer*. 3rd ed. Academic Press, 2013.
- [10] Bruce R. Munson, Donald F. Young, and Theodore H. Okiishi. *Fundamentals of Fluid Mechanics*. 7th ed. Wiley, 2013.
- [11] OMICS International. *Three-Pass Shell Boiler with Rear-Mounted Economizer*. Figure illustrating a three-pass shell boiler with economizer. OMICS International. 2017. URL: <https://www.omicsonline.org/publication-images/innovative-energy-policies-Tube-Steam-Boiler-7-193-g001.png> (visited on 01/09/2026).
- [12] Spirax Sarco. *Shell Boiler Labeled Stages*. Accessed via Spirax Sarco Learn About Steam. Spirax Sarco. 2024. URL: <https://content.spiraxsarco.com/-/media/spiraxsarco/global/learn-about-steam/3---the-boiler-house/shell-boilers/fig-3-2-4.ashx> (visited on 01/09/2026).
- [13] P. K. Swamee and A. K. Jain. “Explicit Equations for Pipe-Flow Problems”. In: *Journal of the Hydraulics Division* 102.5 (1976), pp. 657–664.

- [14] Wolfgang Wagner and Andreas Pruss. *The IAPWS Industrial Formulation 1997 for the Thermodynamic Properties of Water and Steam*. IAPWS-IF97 Official Release. International Association for the Properties of Water and Steam (IAPWS), 1997.
- [15] Frank M. White. *Fluid Mechanics*. 8th ed. McGraw-Hill, 2016.